8-9-2014

Physical and Magnetic Properties of Magnetic Nanoparticle Arrays

Abdul Rahman Mohtasebzadeh
University of South Carolina - Columbia

Physical and Magnetic Properties of Magnetic Nanoparticle Arrays

by

Abdul Rahman Mohtasebzadeh

Bachelor of Science
Herat University, 2008

Submitted in Partial Fulfillment of the Requirements

for the Degree of Master of Science in

Physics

College of Arts and Sciences

University of South Carolina

2014

Accepted by:

Thomas M. Crawford, Director of Thesis

Yanwen Wu, Reader

Lacy Ford, Vice Provost and Dean of Graduate Studies

Dedication

To my family and beloved country

Acknowledgments

This project would not have been possible without the support of many people. I would like to express my deepest gratitude to my advisor, Dr.Thomas Crawford, for his excellent guidance, caring, patience, and providing me with an excellent atmosphere for doing research. Also thanks to the reader of this thesis, Dr.Yanwen Wu, who offered guidance and support. I want to have a special thanks to Dr. Richard Webb, for supporting my research and giving me opportunity to use his excellent research equipments. In addition, I would like to express the deepest appreciation to Dr.Longfei Ye, who trained me to use different laboratory equipments and always guided me to the right direction. I would like to thank my family for their support from thousand miles during my entire academic journey. Finally, I thank all my friends, colleagues and professors for supporting me and encouraging me with their best wishes.

Abstract

Using Scanning Electron Microscope (SEM) , Atomic Force Microscope (AFM) and Vibrating Sample Magnetometer (VSM) I studied magnetic-field directed self-assembly of magnetic nanoparticles into patterned arrays on the surface of perpendicular magnetic recording media. A controllable machine was used to coat super paramagnetic nano particles onto the surface of perpendicular recording media for different time intervals. Self assembled nano particles on the surface of the media, were transferred to a polymer layer to observe physical properties. Results from imaging shows that the average width and height of arrays is increasing as a function of time. Width of arrays varies with assembly time from 149nm at 5 minutes to 525nm at 120 minutes. Similarly, height changes from 13nm at 5 minutes to 37nm at 120 minutes. Therefore the pattern aspect ratio changes from 10:1 at 5 minutes to 14:1 at 120 minutes. For large widths compared with pattern spacing, interactions appear as a slope change in VSM hysteresis loops. Results suggests that there is a significant slope change as the coating time increases and there is a local magnetic particle-particle interaction.

Table of Contents

List of Tables

List of Figures

Chapter 1

Motivation and Introduction

Magnetic interaction in nano-particles arrays is of interest not only in physics but also in other fields such as chemistry, engineering, electronics, medicine, and so on [18] [13] [25] [14]. The main focus of this thesis is the study of magnetic interactions between self-assembled particles on the surface of perpendicular media, specifically the width and height growth of self-assembled particles as a function of assembly time, and their interaction once external field is applied. Perpendicular magnetic recording media directs magnetic nano particles to self assemble onto lines that are equally spaced. These lines are then transferred to a flexible polymer layer in order to study their physical properties [10]. This method not only makes physical measurements easier but also provides a low-cost, polymeric diffraction grating with high precision.

The First chapter discusses some related theoretical topics behind the experimental measurements. It is important to understand basic magnetism in order to explain magnetic nano particles properties. It is also important to understand different kinds of magnetic materials, magnetic media and magnetic recording.

1.1 Review of Basic Magnetics

1.1.1 Magnetic Fields

A magnetic field is a form of matter produced by electric current, and is described by magnetic induction or magnetic flux density $\vec{B}$ which is written in form of *Biot-Savart's* law:

$$\vec{B} = k \iiint \frac{\vec{J}(\vec{\acute{r}}) \times (\vec{r} - \vec{\acute{r}})}{\left|\vec{r} - \vec{\acute{r}}\right|} d^3\vec{\acute{r}} \tag{1.1}$$

Here $\vec{B}$ is the magnetic flux density at position $\vec{r}$, $\vec{J}$ is the current density at position $\vec{\acute{r}}$, $k = \mu/4\pi = 1 \times 10^{-7} H/m$ in the International System (SI) [22].
The magnetic flux within area A which is perpendicular to the induction $\vec{B}$ is:

$$\mathbf{\Phi} = BA \tag{1.2}$$

A magnetic dipole is created by an electrical current flowing in a loop. The magnetic moment of a dipole in (SI) is:

$$\vec{m} = IA \tag{1.3}$$

in this equation I is the current and A is the loop area. The direction of the vector $\vec{m}$ is defined by the right-hand rule. The magnetic induction at position $\vec{r}$ due to a magnetic dipole at the origin is given by:

$$\vec{B} = \frac{\mu}{4\pi}[\frac{3(\vec{\acute{m}} \cdot \vec{\acute{r}})}{r^5}\vec{r} - \frac{\vec{m}}{r^3}] \tag{1.4}$$

Both orbital motion and spin of electrons in molecules can be described as a magnetic dipole. The magnetic moment per unit volume in a material is called magnetization, $\vec{M}$. The spontaneous magnetization (with no applied field) of a non-magnetic material such as air or vacuum is usually zero [22]. The magnetic field, $\vec{H}$, in a material, is defined by:

$$\vec{H} = \frac{\vec{B}}{\mu_0} - \vec{M}. \tag{1.5}$$

For an isotropic uniform material, the constitutive relations that relate magnetic field, magnetic induction and magnetization are:

$$\vec{B} = \mu\mu_0\vec{H}, \vec{M} = \chi\vec{H},\ \mu = 1 + \chi \tag{1.6}$$

Where μ is the (relative) permeability, and χ is the susceptibility. Maxwell's equations that define electromagnetic fields are

$$\nabla \cdot \vec{D} = \rho \tag{1.7}$$

$$\nabla \times \vec{E} = -\frac{\partial \vec{B}}{\partial t} \tag{1.8}$$

$$\nabla \cdot \vec{B} = 0 \tag{1.9}$$

$$\nabla \times \vec{H} = \vec{J} + \frac{\partial \vec{D}}{\partial t} \tag{1.10}$$

These equations are for a dynamic magnetic field. For a static magnetic field, we have

$$\nabla \cdot \vec{B} = 0, \quad \nabla \times \vec{H} = \vec{J}. \tag{1.11}$$

To express in integral form then

$$\oiint \vec{B} \cdot d\vec{S} = 0, \quad Gauss's\ law$$
$$\oiint \vec{H} \cdot d\vec{l} = I, \quad Ampere's\ law$$

Here I is the net current enclosed by the integral loop. One of the most useful results of *Gauss's law* is the absence of magnetic monopoles in nature and the conservation of magnetic flux. *Gauss's law*, can be rewritten

$$\nabla \cdot \vec{H} = -\nabla \cdot \vec{M} \equiv \rho_m \tag{1.12}$$

One can draw a picture of "magnetic charge" density for ρ_m corresponding to the electric charge density. At an interface , magnetic charge density per unit surface is

$$\sigma_m = -\vec{n}_{12} \cdot (\vec{M}_2 - \vec{M}_1), \tag{1.13}$$

where $\vec{n}_{12}$ is the unit vector normal to the interface and pointing from medium 1 to medium 2, Figure 1.1

Figure 1.1 Magnetic charge and Magnetization [22]

The bar has either positive or negative magnetic charges at either end surface[22]. We can now define magnetic field as the gradient of magnetic potential or

$$\vec{H} = -\nabla\phi, \tag{1.14}$$

Where the agnetic potential obeys *Poisson's* equation:

$$\nabla^2\phi = -\rho_m. \tag{1.15}$$

1.1.2 Intermolecular Interactions

Magnetic dipole-dipole interaction

If we consider two bar magnets, the dipole-dipole interaction energy classically depends on the orientation of the magnetic moments [20]. Every magnet produces a field maximum near the poles. The magnetic field of a magnetic dipole

$$\vec{B}(\vec{m},\vec{r}) = \frac{\mu_0}{4\pi r^3}(3(\vec{m}\cdot\hat{r})\hat{r} - \vec{m}) \tag{1.16}$$

When two magnets are placed next to each other, they either repel or attract each other, depending on their orientation. If magnet is placed in a non-uniform field, the pole experiencing the magnetic field will experience a force. Instead of picturing two bar magnets we use magnetic dipoles[22]. The force on a magnetic dipole due to a nonuniform field is

$$\vec{F} = \nabla(\vec{m}\cdot\vec{B}) \tag{1.17}$$

If we consider two dipoles each with magnetic moments $\vec{m}_1$ and $\vec{m}_2$, the force exerted by a dipole with moment $\vec{m}_1$ on the one with moment $\vec{m}_2$ is

$$\vec{F} = \nabla(\vec{m}_2\cdot\vec{B}_1) \tag{1.18}$$

Using expression of field from equation (1.16) we can write,

$$\vec{F}(\vec{r},\vec{m}_1,\vec{m}_2) = \frac{\mu_0}{4\pi r^3}[\vec{m}_2(\vec{m}_1\cdot\hat{r}) + \vec{m}_1(\vec{m}_2\cdot\hat{r}) + \hat{r}(\vec{m}_1\cdot\vec{m}_2) - 5\hat{r}(\vec{m}_1\cdot\hat{r})(\vec{m}_2\cdot\hat{r})] \tag{1.19}$$

If we consider equation (1.20), the strength of the dipole-dipole interaction is not only proportional to magnitudes of the individual dipoles, but also proportional to the distance, the relative orientation and the "spectral overlap of resonances that satisfy the conservation of angular momentum and energy [20].

$$Dipole - dipole interaction \;\propto\; \frac{m_1 m_2}{r^3}(3cos^2\Theta - 1) \tag{1.20}$$

Van der Waals force

The interaction between two non-bonded and un- charged atoms, known as the *Van der Waals* interaction[15].

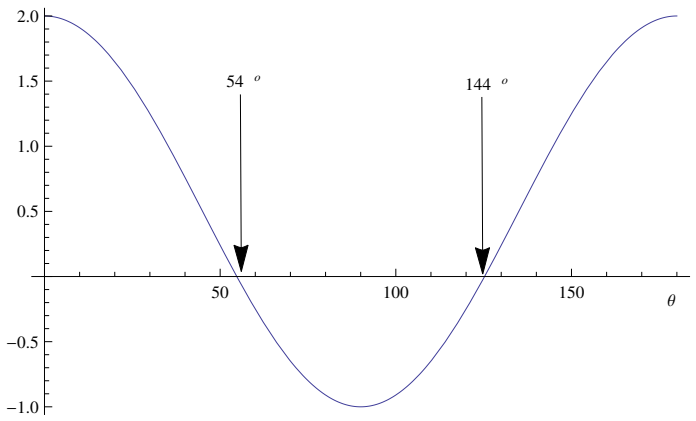

Figure 1.2 plot of the value of $3cos^2\theta - 1$ as a function θ [20]

Van der Waals (VDW) forces explains the attractive or repulsive forces between molecules such as forces between two permanent dipoles [1]. VDW forces are relatively weak compared to covalent bond, however they play an important role in condensed matter physics, polymer sciences, nanotechnology etc [1].

The *Lennard-Jones* potential is an approximation model VDW forces [15]. The very common form of *Lennard-Jones* is described by

$$V_{LJ(r)} = \frac{A}{r^{12}} - \frac{B}{r^6}, \tag{1.21}$$

here, $A = 4\epsilon\sigma^{12}$ and $B = 4\epsilon\sigma^6$, and $\sigma = 0.316555nm$ and $\epsilon = 0.6501696kJ/mol$ are the specific *Lennard-Jones* parameters [19].

When the separation r is very small, the $\frac{1}{r^{12}}$ term dominates, and the potential is strongly positive. Hence this term describes the short range repulsive force caused by the distortion of the electron clouds at small separations. In contrast the $\frac{1}{r^6}$ predominates when the separation r increases in magnitude. Therefore this term describes the long-range attractive tail of the potential between two particles [19].

The minimum force of interaction is $F_{LJ}(r) = -\frac{dV_{LJ}}{dr}$ that is

$$F_{LJ}(r) = \frac{6B}{r^7} - \frac{12A}{r^{13}} \tag{1.22}$$

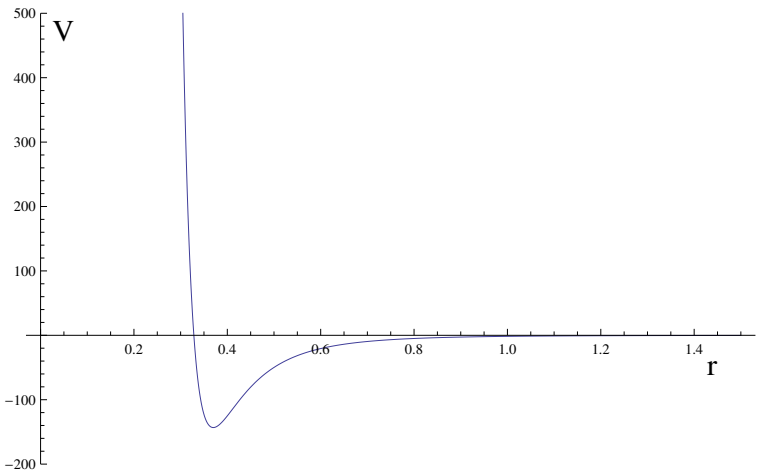

Figure 1.3 Lennard Jones potential as a function of distance

1.1.3 Demagnetization Field

A magnetostatic field inside a magnetic material is often opposite to the magnetization such that it tends to "demagnetize" the latter by superposing the magnetic field due to point magnetic charges [22]. If a point charge q_m is at positive $\vec{r}$, then its magnetostatic field at position $\vec{r}$, is

$$\vec{H} = \frac{q_m}{4\pi} \frac{(\vec{r} - \vec{r})}{\left|\vec{r} - \vec{r}\right|^3} \tag{1.23}$$

The superposition principle leads us to the fact that magnetostatic field produced by a distribution of volume charges ρ_m and a surface charge σ_m is

$$\vec{H}(\vec{r}) = \frac{1}{4\pi} \iiint \rho_m \frac{\vec{r} - \vec{r}}{\left|\vec{r} - \vec{r}\right|^3} d^3\vec{r} + \frac{1}{4\pi} \iiint \sigma_m \frac{\vec{r} - \vec{r}}{\left|\vec{r} - \vec{r}\right|^3} d^2\vec{r} \tag{1.24}$$

or

$$\vec{H}(\vec{r}) = -\frac{1}{4\pi} \iiint \left(\nabla \cdot \vec{M}(\vec{r})\right) \frac{\vec{r} - \vec{r}}{\left|\vec{r} - \vec{r}\right|^3} d^3\vec{r}$$

$$+\frac{1}{4\pi} \iiint \left(\vec{n} \cdot \vec{M}(\vec{r})\right) \frac{\vec{r} - \vec{r}}{\left|\vec{r} - \vec{r}\right|^3} d^2\vec{r} \tag{1.25}$$

The demagnetizing field is therefore a field that is created by the magnetization [22]. This field is proportional to the magnetization by a tensor factor $\overleftrightarrow{N}$.

$$\vec{H}(\vec{r}) = -\overleftrightarrow{N}(\vec{r}) \cdot \vec{M} \tag{1.26}$$

where $\overleftrightarrow{N}$ is a tensor function of position independent of the magnetization [22].

Table 1.1 Some useful definitions and units [22]

Name	Definition	Units
Recording Field	The magnetic field produced by a record head when current is applied	A/m or Oe (oersteds): $1A/m = 4\pi \times 10^{-}3Oe$
Flux	magnetic equivalent of current	Wb (webers) or Mx (maxwells): $1Wb = 10^8 Mx$
Flux Density	Measure of flux per unit area of magnetized material	T (Tesla) $= Wb/m^2$ or G (Gauss); $1T = 10^4 G$
Remanence	The amount of field left by recording	A/m or Oe
Retentivity	A measure of flux remaining after the magnetic field as been removed	T or G
Coercivity	Magnetic field strength required to completely demagnetize a material	A/m or Oe
Saturation Field	The magnetic field necessary to saturate magnetization	A/m or Oe
Saturation Magnetization	The highest magnetization when a magnetic material is completely saturated	emu/cm^3
Remanent Magnetization	The magnetization left after field is removed	emu/cm^3
Coercivity Squareness	Sharpness of the magnetization: $\frac{dM(H)}{dH} = \frac{M_r}{H_c(1-S^*}$	emu/cm^3
Magnetic Susceptibility	Degree of magnetization	emu/cm^3

Materials that are magnetic i.e that can produce magnetic field, are characterized based on their behavior when an external magnetic field is applied. They are mainly divided into the following categories

1.2.1 Diamagnetic Materials

Diamagnetism results from changes in the orbital motion of electrons around atoms. The induced internal field in these materials is directed opposite to the external field. The field creates a force $\vec{F} = q\vec{V} \times \vec{B}$ and changes the direction of centripetal force. The susceptibility of diamagnetic material is negative and varies from -10^{-5} to -10^{-4}. Figure 1.4 shows magnetization of diamagnetic materials versus field and temperature.

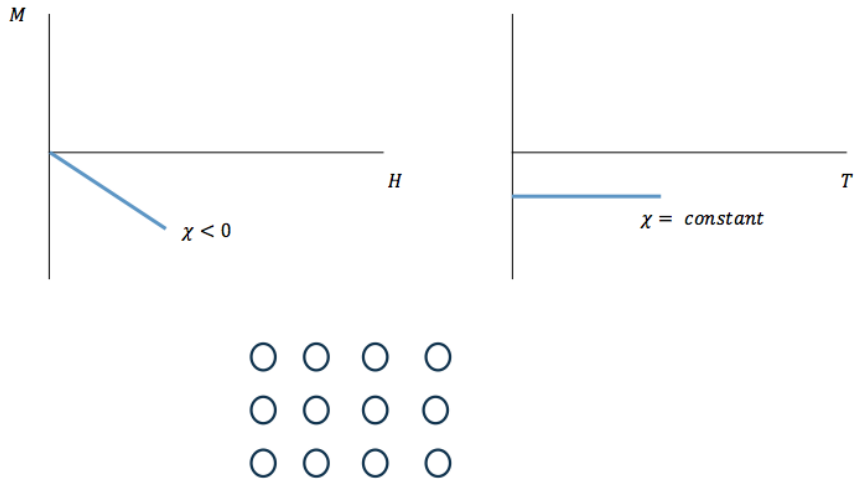

Figure 1.4 M vs H and M vs T for diamagnetic material and magnetic moments have no orientation (net magnetization is zero)

1.2.2 Paramagnetic Materials

Paramagnetism appears when material experiences an external field. It causes due to the exchange interaction of magnetic moment dipoles. The induced magnetic moment produced by field is linear in the field strength and rather weak. Once the field is removed there is no net magnetic moment alignment. Figure 1.5 shows how magnetization of paramagnetic materials changes with field and temperature.

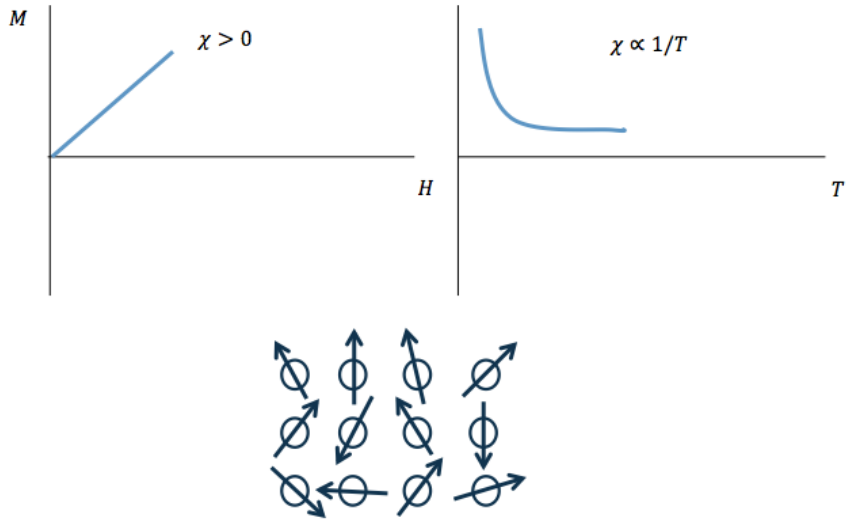

Figure 1.5 M vs H and T for paramagnetic material, magnetic moment in these materials are randomly oriented

The susceptibility of a paramagnetic material is given by *Curie's Law* which says that magnetization is inversely proportional to temperature [7].

$$\vec{M} = C\frac{\vec{B}}{T} = C\frac{\mu\vec{H}}{T} \tag{1.27}$$

In equation (1.27), C is material's specific Curie constant. The proof of this relation is quantum mechanical [11]. Considering a two state spin 1/2 particle aligned with external field, the *Energy* is given by

$$E_0 = m\mu_0 H \tag{1.28}$$

where m is magnetic moment and H is field. The expectation value of magnetic moment is

$$< m >= mP(m) + (-m)P(-m) = 1/Z(me^{\beta mB} - me^{-\beta mB}) \tag{1.29}$$

therefore,

$$< m >= \frac{2m}{Z} Sinh(\beta mB) \tag{1.30}$$

where P is probability of configuration by *Boltzman Factor*, Z is the partition function and $\beta = 1/kT$ [11]. The partition function is defined by

$$Z = \sum_n e^{-E_n\beta} = e^{\beta mB} + e^{-\beta mB} = 2Cosh(\beta B) \tag{1.31}$$

For simple case $< m >= mtanh(\beta mB)$. And the total magnetization is given by

$$M = N < m >= Nmtanh\Big(\frac{mB}{kT}\Big) \tag{1.32}$$

The last equation is known as *Langevin paramagnetic equation* [11]. For relatively high temperatures and low magnetic fields the factor $\left(\frac{mB}{kT}\right)$ is much less than one [7]. Therefore, $tanh\Big(\frac{mB}{kT}\Big) \approx \left(\frac{mB}{kT}\right)$,

$$\vec{M}(T \to \infty) = \frac{Nm^2}{k}\frac{B}{T} \tag{1.33}$$

This relation leads to equation (1.27) with Curie's constant $C = nm^2/k$.

1.2.3 Ferromagnetic Materials

Like paramagnetism, ferromagnets tend to align magnetic moment dipoles when field is applied. The main difference, however, is that even after removing the field they remain aligned and magnetic moment dipoles align themselves to the neighboring ones. The reason is quantum mechanical [22]. The alignment occurs in very small parts of material that are called *domains* [4]. There are many domains that have

different alignments. Domains are visible under a microscopes that can detect magnetization [4]. The number of domains depends on how large a ferromagnetic material is. The boundary between two neighboring domains is called a domain wall or magnetic transition. The atomic dipole moment in ferromagnetic materials has a strong exchange interaction, i.e a field around $10^3 T$ much larger than earth's magnetic field. Figure 1.6 shows magnetization of ferromagnetic material materials versus field and temperature.

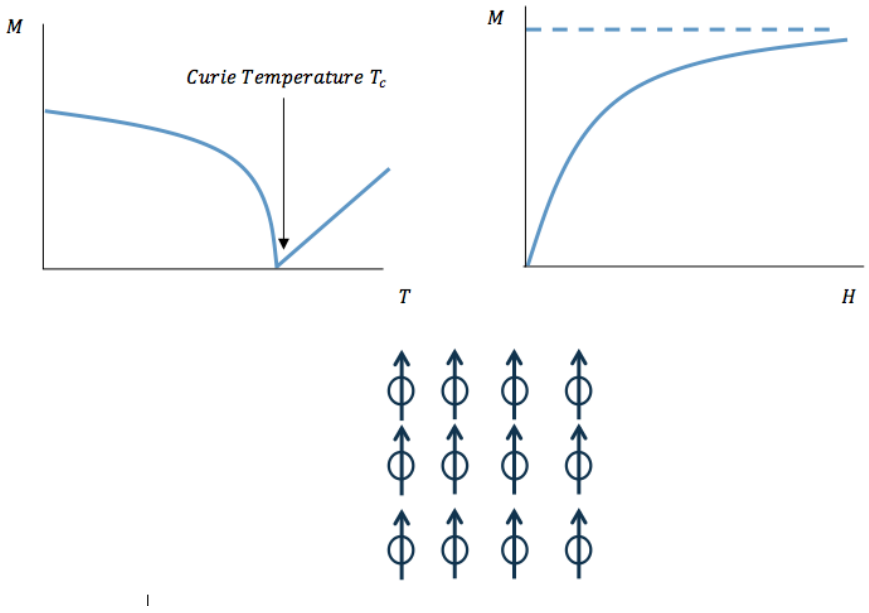

Figure 1.6 M vs H and T for ferromagnetic material, magnetic dipoles are aligned within the domain

Figure 1.6 shows that as H increases M reaches to a saturation. As T increases, M drops to a *Curie temperature*, where the net magnetization of ferromagnetic material is zero (high temperatures breaks the long range ferromagnetic order) The susceptibility of ferromagnetic materials are given by *Curie-Weiss law* that is derived from *Curie's law*

$$\chi = \frac{C}{T - T_c} \tag{1.34}$$

Below the Curie temperature, a ferromagnet usually has a temperature dependent spontaneous magnetization. The spontaneous magnetization arises from magnetic dipoles due to itinerant electrons (free electrons that are not confined to atomic cores) and unclosed atomic electron orbitals [22]. The magnetization of a ferromagnetic material as a function of applied field is dependent on the history of the applied field.

Most of the time the applied field is the same as the internal field of the magnetic material with no demagnetization field, and the hysteresis is an intrinsic property of magnetic material, independent of geometry[22]. For nonzero demagnetization factor, the intrinsic hysteresis will be sheared by an amount determined by the demagnetization factor

$$H_{in} = H_{ex} - N_d \tag{1.35}$$

An intrinsic hysteresis loop $M = M(H_{in})$ will change into a sheared loop

$$M = M(H_{ex} - N_d M) \tag{1.36}$$

The hysteresis loop is symmetric and often described by factors such as coercivity H_c , saturation magnetization M_s and remanence magnetization M_r .

Magnetic materials with coercivity less that $10Oe$ are called soft magnetic materials, and magnetic materials with coercivity larger than $100Oe$ are called hard magnetic materials.

1.2.4 Antiferromagnetic Materials

The neighboring spins in this materials are antiparallel and they can only be noticed at low temperatures [22]. The transition temperature is known as *Neel temperature*. Magnetic susceptibility of antiferromagnetic materials increases as temperature is lowered, as given by the following formula

$$\chi = \frac{C}{T + \theta} \tag{1.37}$$

Below the *Neel* temperature of an antiferromagnet the spins have antiparallel orientations, the susceptibility attains its maximum value at T_N, with a well defined kink in the curve of χ versus T

1.2.5 Ferrimagnetic Materials

Ferrimagnetic materials have populations of atoms with opposing magnetic moments same as antiferromagnetic materials, only the moments are unequal. They hold a spontaneous magnetization below the Curie temperature, and show no magnetic order above this temperature [4]. These materials have high resistivity and anisotropic magnetic properties.

1.2.6 Superparamagnetic Materials

Super-paramagnetism appears in small ferromagnetic or ferrimagnetic nano-particles. In sufficiently small nano-particles, the magnetization can randomly flip direction under the influence of temperature [7]. The typical time between two flips is called the *Néel relaxation time* τ_n.

$$\tau_n = \tau_0 e^{\frac{KV}{k_B T}} \tag{1.38}$$

Here, τ_0 is characteristic of material called *attempt time*, K is the material's magnetic anisotropy energy density and V is volume, and the quantity KV is called *the energy barrier* associated with magnetization moving from its initial easy axis direction, through a hard plane to the other easy axis direction, k_B is Boltzmann constant and T is temperature [7].

The state of superparamagnetic nanoparticles depends on measurement time [7]. If the measured time is greater than relaxation time then nano particle magnetization will change the orientation during measurement. If the measurement time is much less than the relaxation time the magnetization will not change the orientation. The temperature in which measurement equals the time and relaxation time is called the blocking temperature, T_B.

$$T_B = \frac{KV}{k_B ln(\frac{\tau_m}{\tau_0})} \tag{1.39}$$

Finite magnetic moments of superparamagnetic materials are aligned with an external magnetic field and become zero after the field is removed[4]. If we consider non-interacting nano particles, the magnetization $M(H)$ at a magnetic field H is

$$\frac{M(H)}{M_S} = coth\Big(\frac{\mu_0 H}{k_B T}\Big) - \frac{k_B T}{\mu_0 H} = L\Big(\frac{\mu m H}{k_B T}\Big) \tag{1.40}$$

where , $\mu_0 = 4\pi \times 10^{-}7H/m$, and L is called *Langevin Function*. It can also be written in following form

$$\frac{M(H)}{M_S} = coth(a) - \frac{1}{a} \tag{1.41}$$

The expression on the right is abbreviated to $L(a)$

$$L(a) = \frac{a}{3} - \frac{a^3}{45} + \frac{2a^5}{945} - ..... \tag{1.42}$$

where $a = \frac{\mu_0 m H}{k_B T}$. For low fields a is linear and small.

Figure 1.7 shows the Langevin function. For values $L(a) = a/3$ the graph is linear [4].

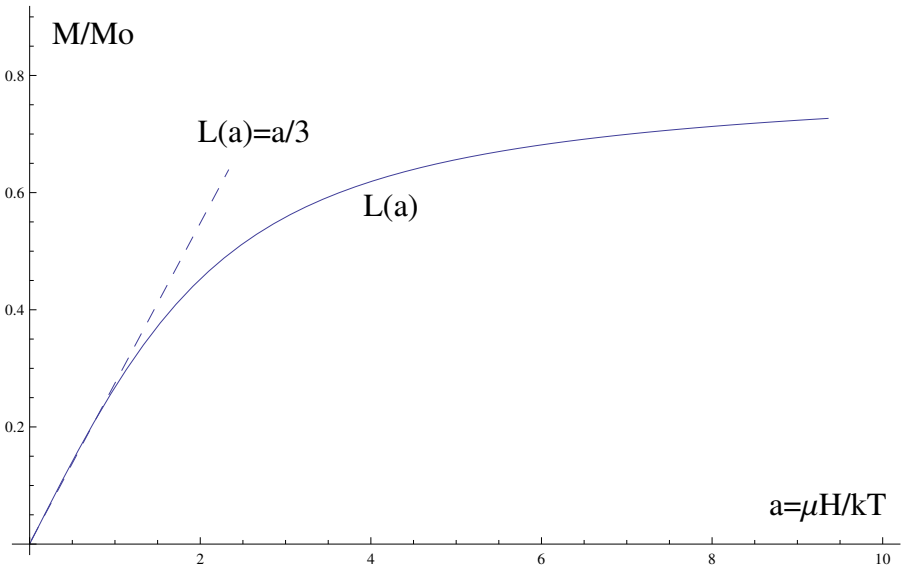

Figure 1.7 Langevin Function [4]

1.3 Anisotropy

Anisotropy is the dependence of magnetic properties on the direction in which they are measured [4]. For example it's easy to magnetize a magnetic material when field is applied along a specific direction known as easy axis and it's unfavorable to magnetize in a direction called hard axis.

Magnetocrystalline Anisotropy

Due to crystal symmetry, certain electron orbitals are not spherical. In the presence of a weak spin-orbit coupling, magnetization (antiparallel to spin) will be coupled to electron orbitals and thus have a lowest or highest energy along certain symmetry axes [4]. For cubic crystals, the magneto crystalline energy per unit volume can be generally expressed as:

$$E = K_0 + K_1(\alpha_1{}^2\alpha_2{}^2 + \alpha_2{}^2\alpha_3{}^2 + \alpha_3{}^2\alpha_1{}^2) + ..., \tag{1.43}$$

Here α_i are the direction cosines of the magnetization with respect to crystal

axes. K_i are constants that have specific values for different crystal structures in different materials [22]. For Hexagonal crystals, the magneto crystalline energy per unit volume can be generally expressed as

$$E = K_0 + K_u sin^2\theta + K_{u2} sin^4\theta + ..., \tag{1.44}$$

where θ is the angle between the magnetization and the [0001] c-axis.In Co for instance, $K_{u2} = 15 \times 10^6 J/m^3$ and $K_u = 45 \times 10^6 j/m^3$.

Shape Anisotropy

Due to the magneto static interaction between magnetization $\vec{M}$ and its own demagnetization field $\vec{H}_d$, a magnetic material possesses so called demagnetizing energy per unit volume:

$$E = -1/2\mu_0 \vec{M} \cdot \vec{H}_d \tag{1.45}$$

The demagnetizing energy is always positive or zero. The magnitude of demagnetizing energy depends on the shape of material. For a very long cylinder along z-axis for example, the demagnetizing factors are $N_1 = N_2 = 1/2, N_3 = 0$ [22]. The shape anisotropy energy per unit volume is

$$E = 1/4\mu_0 M^2 sin^2\theta \tag{1.46}$$

Where θ is the angle between the magnetization and the z-axis. Therefore, the cylindrical axis is the easy axis [22]. Similarly for a thin film perpendicular to the z-axis, the demagnetizing factors are $N_1 = N_2 = 0, N_3 = 1$ and anisotropy energy per unit volume is

$$E = 1/2\mu_0 M^2 cos^2\theta \tag{1.47}$$

Here the thin film normal axis is the hard axis [22].

Magnetic recording (or magnetic storage) is storage of information on a magnetized material (medium), such as Hard Disk Drives (HDD), Compact Disks, Tapes and so on. Recording can happen in different patterns of magnetization in some magnetizable media. The recording relies on the magnetization of the media by a magnetic field, derived from an electrical signal, provided by a "Recording Head" [16].

1.4.1 Recording head

The head produces a field that alters the magnetization of the medium so that it aligns with the imposed field. The head consists of a torroidal ferromagnetic core wrapped with wires (the "coil") with a small air gap Since the gap in the head has a high reluctance, the field fringes at the gap and magnetizes media as it passes by.

The recording head has a soft magnet core with cross section A_c with the gap of constant area A_g. Neglecting the fringe field near the gap, Magnetic flus Φ is constant and defined as

$$\Phi = B_c A_c = B_g A_g, \tag{1.48}$$

B_c is magnetic flux density in core and B_g is magnetic flux density in gap. From *Ampere's* law one can write,

$$NI = H_c l_c = H_g g, \tag{1.49}$$

N is the number of coil turns, I is the write current, H_c is magnetic field in the magnetic core (not coercivity), l_c is the length of the magnetic core and g is the length of the head gap.

By substituting magnetic field by magnetic flux density using equation (1.6) relation (1.22) becomes

$$NI = \frac{B_c}{\mu_c \mu_0} l_c + \frac{B_g}{\mu_0} g = \Phi\left(\frac{l_c}{\mu_c \mu_0 A_c} + \frac{g}{\mu_0 A_c}\right) \tag{1.50}$$

Here, μ_c is the permeability of magnetic core.

1.4.2 Magnetic Recording Medium

a magnetic medium consists of different parts. As an example we consider thin-film in most dominant disks presented in Figure bellow.

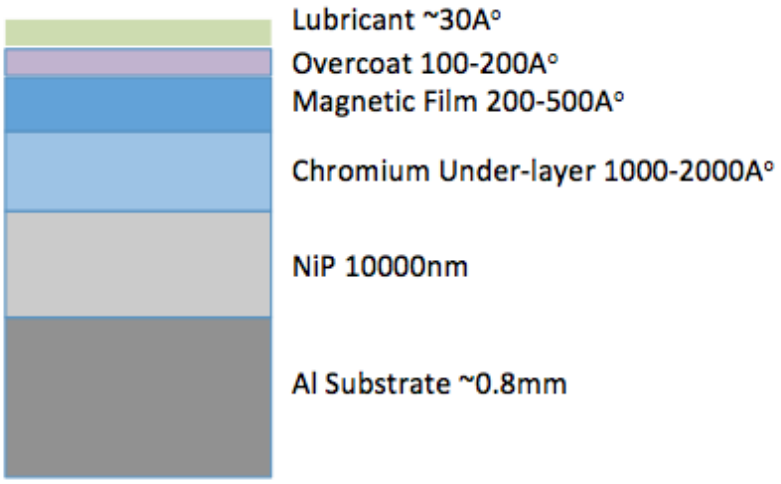

Figure 1.8 parts of magnetic media [22]

The first layer is aluminum substrate coated with NiP to make the disk rigid and smooth. Next layer is Chromium under-layer which acts as a controller of magnetic properties of the magnetic recording layer. The magnetic part that mostly is Cobalt based alloy is covered by carbon overcoat and lubricant. The speed of under the head must be greater than 5000 RPM and the distance should be around 38 nanometer [22].

1.4.3 Magnetic field of a single transition

The field inside a magnetized medium is created by bound currents [22]. This magnetic field can be computed by equation (1.19). The magnetic medium extends horizontally in (x, y) plane, and for a single step transition below, the following relation for M as a function of position holds

$$M(x) = \begin{cases} -M_r \quad for \quad x < 0 \\ \\ M_r \quad for \quad x > 0 \end{cases} \tag{1.51}$$

The surface charge density $\sigma_m = -2M_r$ at the transition center $x = 0$, and extends from $-\frac{\delta}{2} < y < \frac{\delta}{2}$, where δ is the the thickness of the media and M_r is remanence magnetization of magnetic media [22]. From equation (1.19), thefield components for x and y are

$$H_x(x, y) = -\frac{M_r}{\pi}\Big[\arctan\Big(\frac{y + \frac{\delta}{2}}{x}\Big) - \arctan\Big(\frac{y - \frac{\delta}{2}}{x}\Big)\Big] \tag{1.52}$$

$$H_y(x, y) = -\frac{M_r}{2\pi}\ln\Big[\frac{(y + \frac{\delta}{2})^2 + x^2}{(y - \frac{\delta}{2})^2 + x^2}\Big] \tag{1.53}$$

Basically there are two ways of recording a magnetic media will be discussed in following sections, known as Longitudinal Recording and Perpendicular Recording.

1.4.4 Longitudinal Recording

In longitudinal recording the medium magnetization is parallel to the disk surface. In this type of recording the magnetization of each data bit is aligned horizontally with respect to disk drive's spinning platter (a circular disk on which magnetic data are basically recorded [8]. The field between two adjacent bits with opposing magnetizations are separated by a transition region[22]. The magnets representing each bit are lined up end-to-end along circular tracks in the plane of the disk. Considering the highest density bit pattern of alternating *ones* and *zeros*, adjacent magnets end up

from north pole to north pole and south pole to south pole [8]. This causes repulsion between them that leads to instability against thermal fluctuation.

1.4.5 Perpendicular Recording

Unlike longitudinal recording the magnetization in perpendicular recording is aligned vertically relative to disk drive's platter. Bits do not directly oppose each other, therefore the need for transition packing is significantly reduced which allows bits to pack closer with sharper transition signals[22]. In this model adjacent magnets (bits) stand in opposite directions next to each other i.e north pole next to south pole, and therefore tend to attract each other with more stability [9].

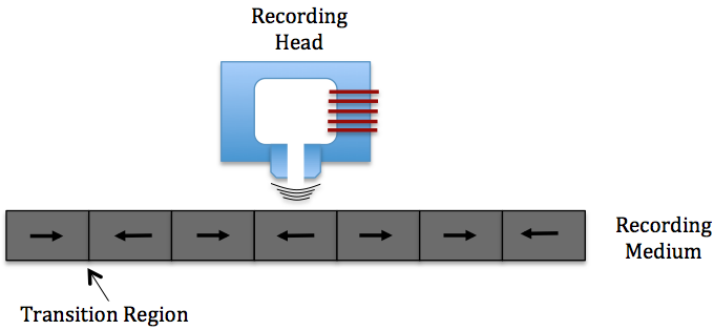

Figure 1.9 Longitudinal recording

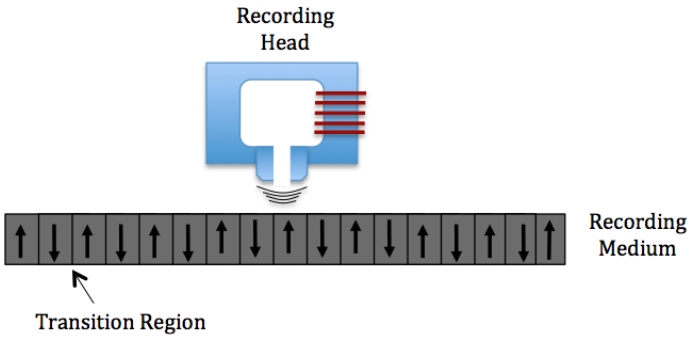

Figure 1.10 Perpendicular recording

Chapter 2

Instruments for Measurements

This section will introduce the experimental instruments that were used for my measurements. There are different ways to measure magnetization such as Alternating Gradient Magnetometer AGM and Vibrating Sample Magnetometer [4]. To observe the selfassembly of magneto nanoparticles, especially width growth of nano particles within the transition patterns, one has to observe them with a scanning electron microscope (SEM). However, to see the height of the selfassembled particles atomic force microscopy (AFM) is the best instrument.

2.1 Vibrating Sample Magnetometer

Vibrating Sample Magnetometer (VSM) is a scientific apparatus that is used to measure magnetic properties of different materials. It was invented by Simon Foner in mid 1950's [6]. VSM detects a sample moment via a change in flux through a coil as the sample vibrates through it [4]. The Quantum Design Physical Property Measurement System (QD-PPMS) VSM, vibrates the sample along the applied magnetic field using a linear motor that creates sinusoidal vibrations at 40Hz [5]. In general VSM works based on Faraday's Law of Induction which states that the change in magnetic field produces an electric field [21]. For magnetic sample, some constant magnetic field will magnetize it. The magnetic dipole moment of the sample creates a changing magnetic field around the sample, known as magnetic stray field. The induced voltage is given by:

$$V_{coil} = \frac{d\Phi}{dt} = \left(\frac{d\Phi}{dz}\right)\left(\frac{dz}{dt}\right) \tag{2.1}$$

Where Φ is the magnetic flux enclosed by the pickup coil and z is the vertical position of the sample with respect to the coil and t is the time[21]. For a sinusoidally oscillating sample position the voltage is based on the equation

$$V_{coil} = 2\pi f C m A sin(2\pi f t). \tag{2.2}$$

In this equation A and f are amplitude and frequency of oscillation respectively, m is the DC magnetic moment of the sample and C is a coupling constant[21]. Different parts of VSM are shown in figure below

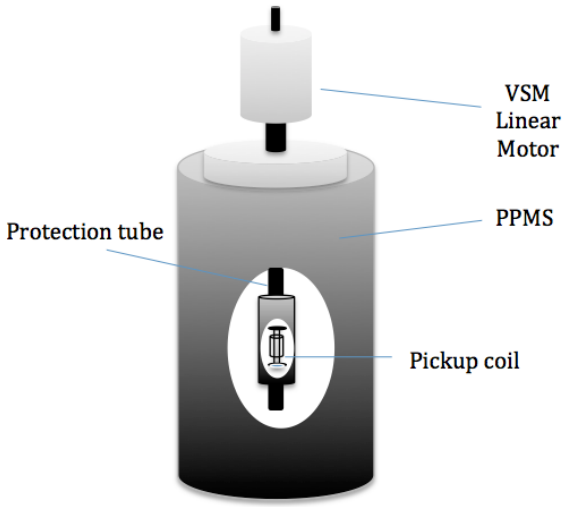

Figure 2.1 Parts of VSM [5]

Once the strength of the constant magnetic field is set, the sample begins to vibrate. The input signal that is received from the probe is changed to a value of magnetic moment of sample [6]. Then the strength of magnetic field changes to a new value. Once again the signal is changed to the value for the magnetization of the sample and finally the constant magnetic field changes over a previously modified range.

2.2 Scanning Electron Microscope

Scanning Electron Microscope (SEM), scans a focused electron beam over a surface of a target to create an image. For the measurement of nanoparticle properties and see how nanoparticle patterns grow with time, it is important to have high resolution images. In SEM, electrons are produced by filament, usually tungsten [17]. Electrons then accelerated towards the sample. During this process electrons are focused by different lenses and apertures. The position of the beam is controlled by coils that allow the beam to be scanned over the sample surface. The incident electron beam will interact with the sample surface sample and produce back-scattered secondary electrons which are collected by detector [17]. Figure 2.2 shows the SEM structure.

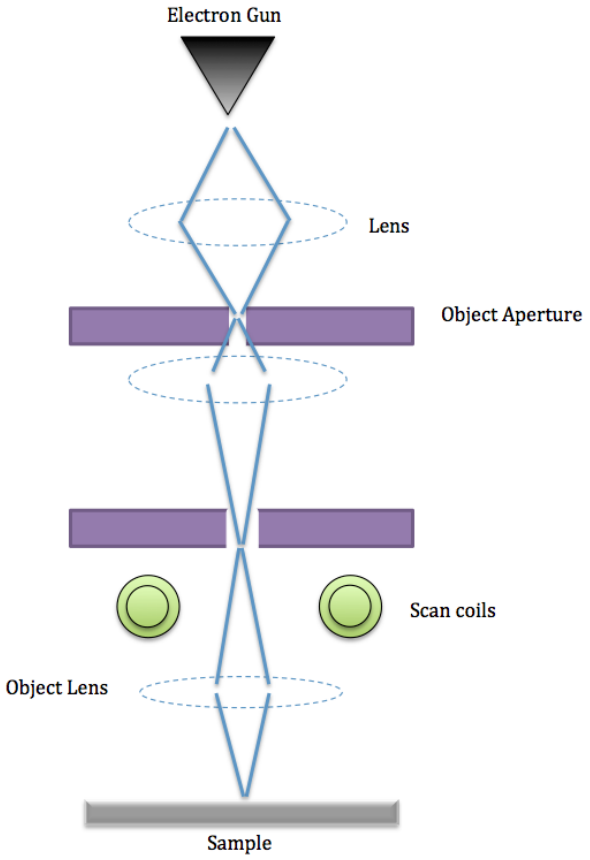

Figure 2.2 Parts of SEM [17]

2.3 Atomic Force Microscope

Atomic Force Microscopy (AFM) is a high resolution scanning microscope that is able to demonstrate resolution on the order of a nanometer. AFM belongs to a series of scanning probe microscopes invented in the 1980s [12]. AFM scans the sample with a sharp tip, which is mounted on a cantilever spring. When the tip goes over the sample surface, there will be an interaction force that can be controlled by the deflection of cantilever. A topographic image of the sample is obtained by plotting the deflection of the cantilever Z_c versus its position on the sample (position of piezo Z_p) [2]. The different parts of the AFM is shown in figure below.

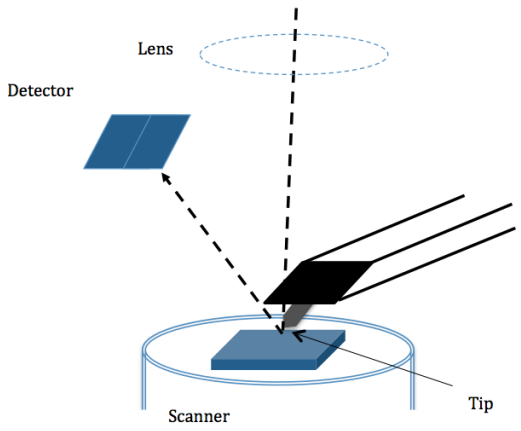

Figure 2.3 Parts of AFM [2]

In AFM, either the sample moves up and down or the cantilever does. This movement is controlled by the piezoelectric translator[2]. The measurement can be operated in air, vacuum, different gases, or liquid. The force on the cantilever is

$$F = Z_c K_c, \tag{2.3}$$

where K_c is spring constant of cantilever. The deflection is calculated by applying a laser beam to the tip of the cantilever. Once force is applied to the probe, it makes

the cantilever bend. For a rectangular shaped cantilever the change in deflection over position is given by

$$\frac{dZ_c}{dX} = \frac{6FL^2}{Ewt_c^3} \tag{2.4}$$

$$Z_c = \frac{4fL^3}{Ewt_c^3} \tag{2.5}$$

Where w , L and t_c are width, length and thickness of cantilever respectively and E is the Young's modulus of the cantilever material. Based on these equations, the movement of cantilever should be very slow.

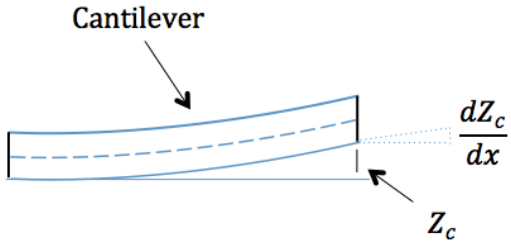

Figure 2.4 Figure of cantilever bent while touching the surface of a sample [2]

The mechanical properties of cantilever play important role on its performance, it is usually made of silicon or silicon nitride. Critical properties are thespring constant k and resonance frequency ν [3]. For rectangular cantilevers the spring constant is:

$$K_c = \frac{F}{Z_c} = \frac{Ewt_c^3}{4L^3} \tag{2.6}$$

Cantilever movement is described by the following equation of motion

$$m\frac{d^2Z_{c(t)}}{dt^2} + \gamma_D\frac{dZ_{z(t)}}{dt} + k_cZ_{c(t)} = F(t) \tag{2.7}$$

$$m = 0.24247m_c + m_t$$

where m is the effective mass of cantilever with $m_c = wt_cL\rho$ actual mass of cantilever and m_t mass of the tip. The solution for this equation is described by a sinusoidal function, $F = F_0 sin(wt)$.

2.4 Stir Coating Machine "Doodad"

There are different ways to coat nanoparticles onto the surface of magnetic media. One can simply put the media inside the nanoparticle solution or attach it to a mount and stir it inside the solution. It is also possible to put a specific amount of nano particle solution on the surface of the media. To study magnetic interactions with good precision, special equipment was designed by our group that can stir any magnetic media in nanoparticle solution. This device, "The Doodad", was programmed with LabView and has a motor that provides different speeds for stirring. Figure 2.5 shows different parts of the Doodad.

The user can program different speeds and set the coating time. The maximum speed is $25 degrees/sec$. A sample holder is attached to a rotating ring and the media has to be mounted in such a way that it is centered during the motion, always parallel to the tangential vector of the rotating ring.

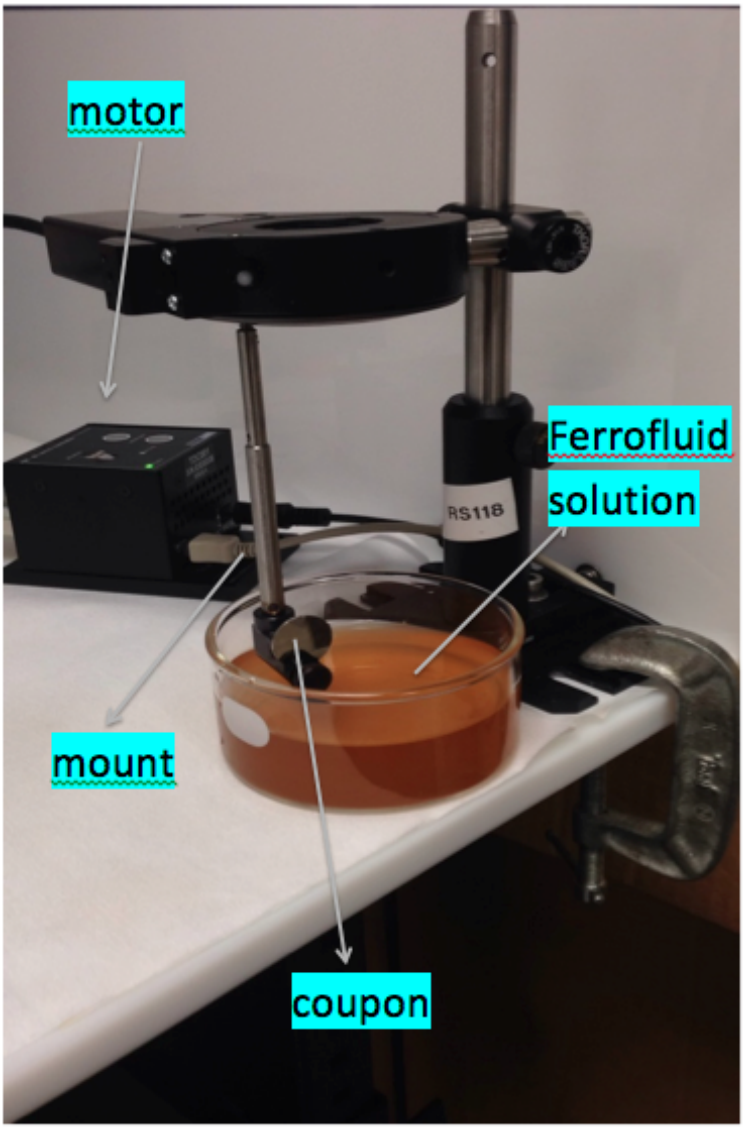

Figure 2.5 Spin string machine, "The Doodad"

Chapter 3

Experimental Procedure for Measuring Magnetic Nano-particle Properties

This chapter explains the method used to coat nanoparticles on the surface of magnetic media and to transfer the nanoparticles from the media to a thin polymer layer to measure their magnetic properties. The recording media used for experiments is a magnetically-recored perpendicular coupon. It is a round shape with 15.12mm diameter and 0.78mm thickness. Colloidally suspended nano-particles are coated on the surface of this coupon using the ultra-high field gradients near the magnetic medium surface [10]. The coated coupon is then studied with AFM and SEM to determine height and width of assembled nanoparticles respectively. Then, self-assembled nano particles are peeled from the surface of the media by a thin polymer film for magnetometry measurements.

3.1 Preparing Nano-particles Solution

To coat magnetic nanoparticles onto the surface of the perpendicular recorded media, a base nanoparticle suspension has to be made. A specific amount EMG707 ferrofluid is suspended into Deionized Water (DI). EMG707 (anionic surfactant) ferrofluid, has 0.001 percent volume concentration of around $13nm$ diameter nanoparticles [23]. The solution is made using the following steps. Two empty $50ml$ falcon tubes are used to make a mixture of $2 \times 25ml$ DeIonized Water (DI water) , $2 \times 25\mu l$ of EMG-707 and $2 \times 2187,5\mu l$ of PBS (Phosphate Buffer Saline) [23]. That is the amount fills a beaker

of solution for coating the disk coupon with the Doodad. In an empty 50ml falcon tube, first $20ml$ of DI water is added with digital pipetter adjusted by pulling and releasing the triggers, and then $25\mu l$ of the EMG-707. To get the EMG-707 mixed with DI water, shake for 10 second using Vortex-Gene touch mixer. Then another $20ml$ of DI water added to the mixture and again vortexed for 10 seconds. At last $10ml$ DI water is added and followed by 10 seconds of vortex. Finally, $2187,5\mu l$ of Phosphate Buffer Saline (PBS) is added to the mixture and vortexed for another 10 seconds. This procedure is repeated for another $50ml$ falcon tube.

PBS enhances the self-assembly of nanoparticles. The small volume of the buffer which has a neutral pH increases the diffraction efficiency dramatically. If the amount of PBS is increased then the grating self-assembly efficiency decreases. This small volume of PBS will not cause aggregation of nanoparticles and will keep the particles remain colloidally suspended in the fluid. However, it is very important to start coating right after PBS is added. If PBS stays in solution for long times, the nanoparticles will start to aggregate [24].

3.2 Coating Nanopartiles Solution

To coat nanoparticles, the surface of the magnetic media has to be clean. To clean the coupon, first it is placed on a clean wiper under the hood. Cotton swabs are used to remove dust and other particles from its surface. First, the coupon is sprayed three times by DI water and each time it has to be wiped gently by a clean cotton swab. The remaining DI water is removed from the coupon's surface by blow drying using Nitrogen gun. It is then sprayed with methanol and cleaned by another clean cotton swab. This process is repeated until the surface of the coupon is completely clean. To very that the surface of the coupon is clean enough, it is useful to check the coupon with a dark field optical microscope.

The coupon has a visible reference line which is parallel to the recorded transition

tracks on the surface of the media. The clean coupon is then mounted on the Doodad's mount such that the reference line is parallel to the horizontal plane as shown in figure 3.3.

Once the coating process is completed, the Doodad will automatically stop and the sample immediately removed from the solution and dried. My experience is that once the coupon is dried, some crystals inside the base suspension will remain as dirt on the surface of the coupon. Therefore, it's always good to have another container with DI water to clean crystals off. However, one has to be very careful not to wash the coated particles away. It is best to dip the coupon horizontally in the surface of the water and take it out vertically but not shaking. Depending on the coating time, one can let the coupon be in the water for different times. For instance, for 5 minutes coating I kept the coupon inside DI water for 1-2 seconds and for 2 hours coating I kept it for 5-6 seconds. After cleaning, coupon has to remain vertical on a clean wiper for 10-15 minutes.

Once the coupon is coated and dried, the self-assembled magnetic particles should form a diffraction as shown in Figure 3.1.

3.3 Grating Pattern Transfer

In order to measure the magnetic properties of nanoparticles self-assembled on the surface of the media a liquid polymer solution was made and spin-coated onto the coupon's surface. Fresh Diskcoat 4220 from General Chemical Corp., is diluted with DI water by ratio of 4:1 [23]. It is good to mix 4ml of Diskcoat polymer with $1ml$ of DI water and use it for maximum 1 week after dilution. If the Diskcoat 4220 is aged, it's better to use it without adding DI water. About $500\mu l$ of liquid polymer solution is poured onto the surface of the coupon and spun for 20 seconds at 2000 RPM. The polymer coated coupon is then left under the hood for 25 minutes at room temperature. The thin film polymer will stick onto the surface of the coupon and

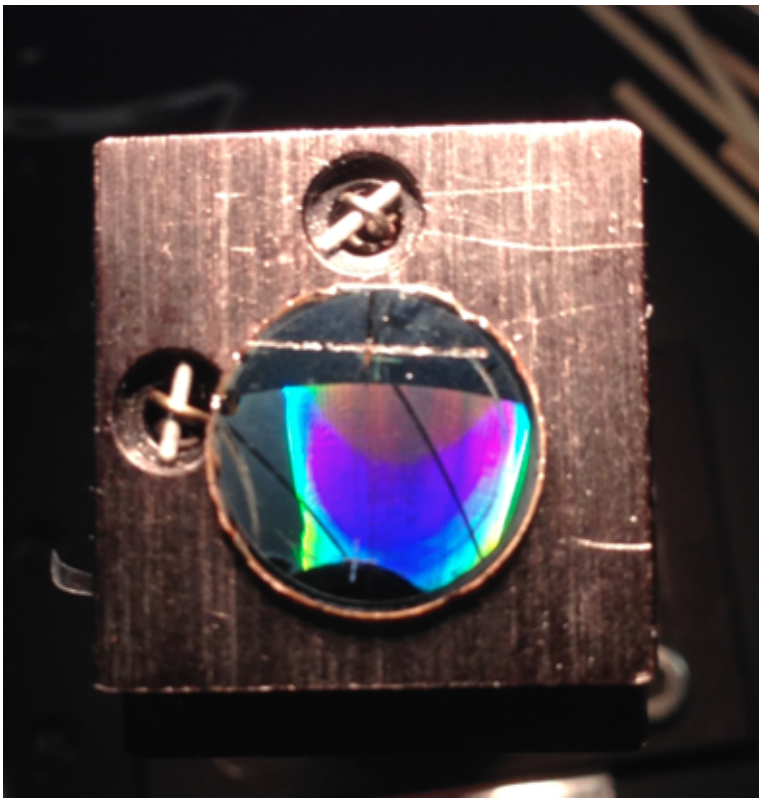

Figure 3.1 Coated coupon

grab the self-assembled nano-particles.

To peel the polymer layer from the surface of the coupon, one can use either double sided tape or reinforcement round tapes (which perfectly matches the diameter of the coupon). Double sided tape has advantage of being easier to mount on the VSM sample holder but it is thicker than reinforcement tape making it hard to see particles with the optical microscope. Figure 3.2 shows the real peeled double sided tape, notice that the diffraction is visible even after peeling. Figure 3.3 shows the whole process from coating nanoparticles using the Doodad and peeling with double sided tape to mounting the peeled tape on VSM sample holder.

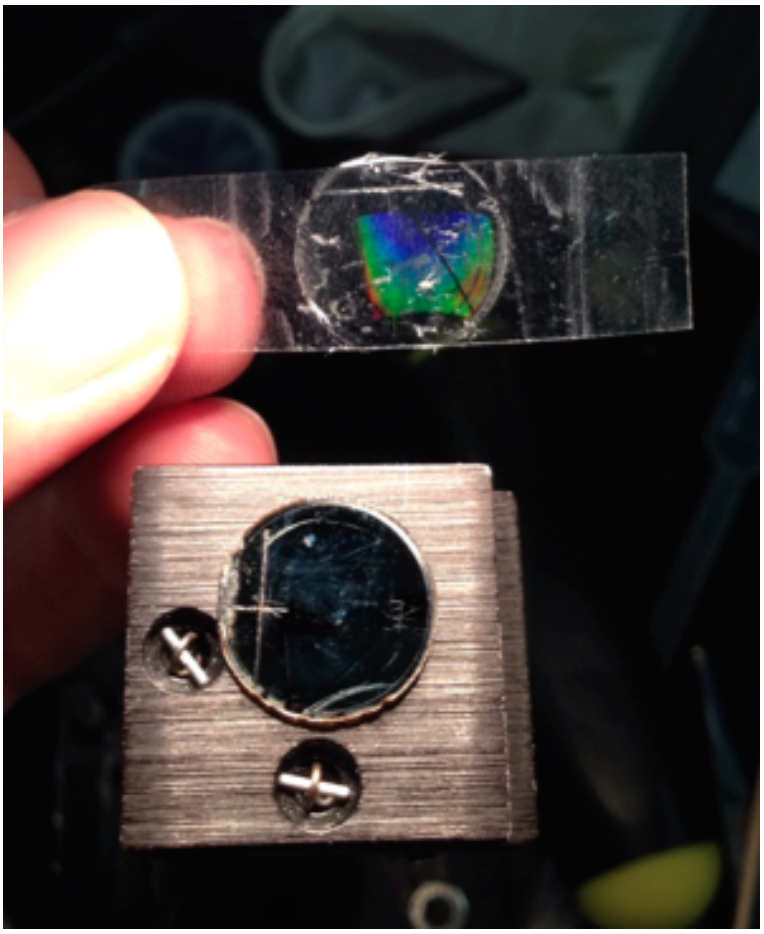

Figure 3.2 Pealed polymere film via double sided tape

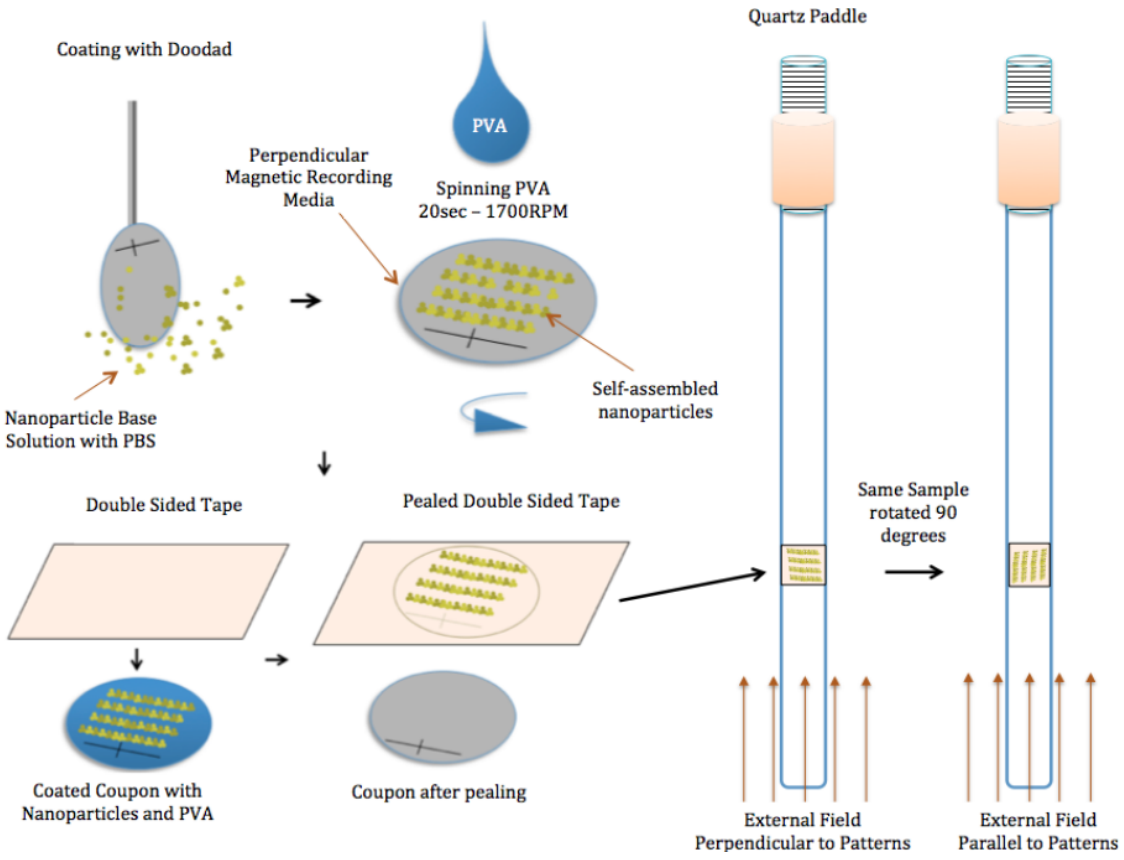

Figure 3.3 Process of coating nanoparticles, pealing polymer film and mounting on VSM quartz paddle

Chapter 4

Results and Discussions

4.1 Pattern Width Growth

The growth of nanoparticle arrays depends on the coating time. Nanoparticle array growth can be observed with the optical microscope. Figure 4.1 compares the width growth of arrays for 15 minutes coated perpendicular media (coupon) and 2 hours coated coupon observed under the optical microscope.

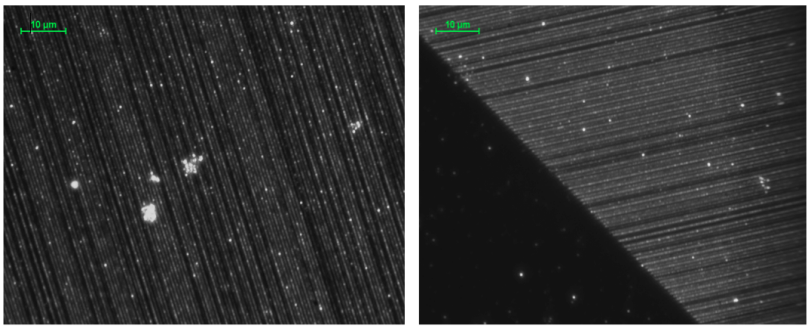

Figure 4.1 Image of 15 minutes coated coupon (left) and 2 hours(right) with 100x lens magnification of optical microscope

As shown in figure 4.1 the spacing between patterns is noticeable, but not very clear and it is hard to determine the width difference as a function of coating time. To observe and calculate width growth accurately, one has to use Scanning Electron Microscope. The coupon was coated 5 times for different time intervals. Then the coupon was dried and studied with SEM.

Figure 4.2 shows SEM image of coupon coated for 5 minute.

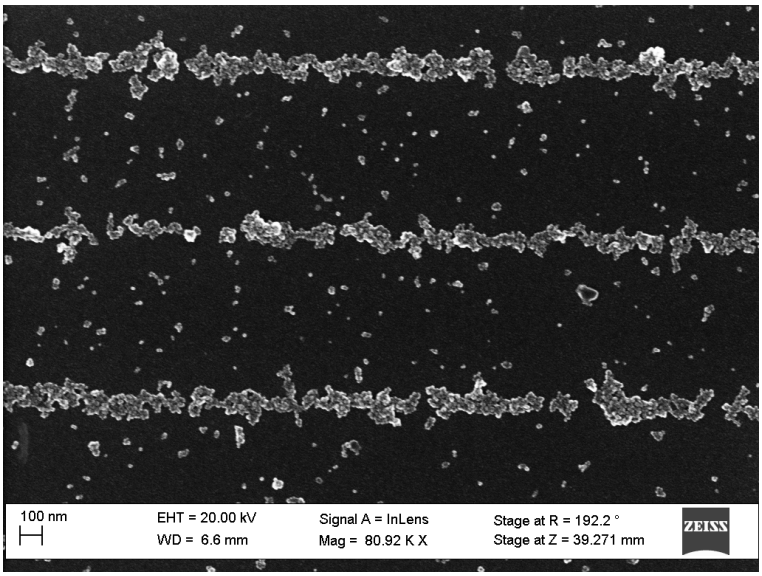

Figure 4.2 SEM image of coupon coated for 5

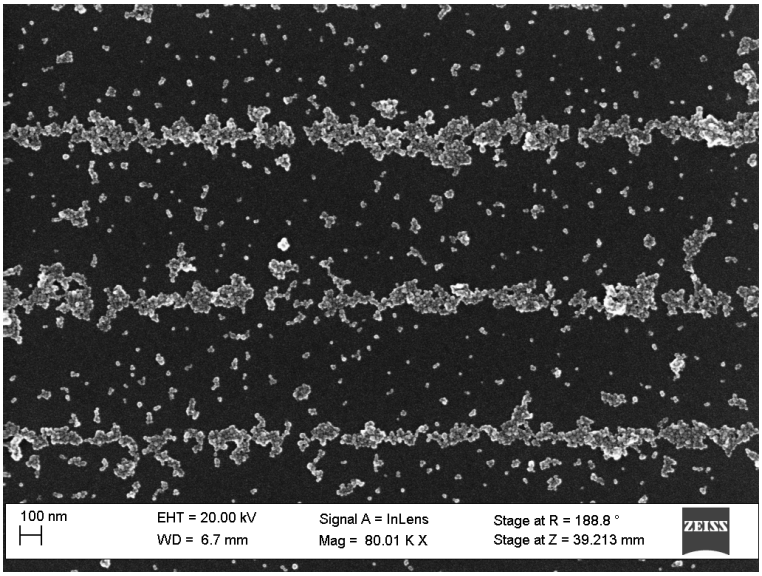

Figure 4.3 SEM image of coupon coated for 15 minutes

Figure 4.3 shows SEM image of coupon coated for 15 minute. It is noticeable that the number of particles in-between arrays in 15 minutes is more than in 5 minutes. Also for both 5 and 15 minutes there are gaps between particles within the patterns.

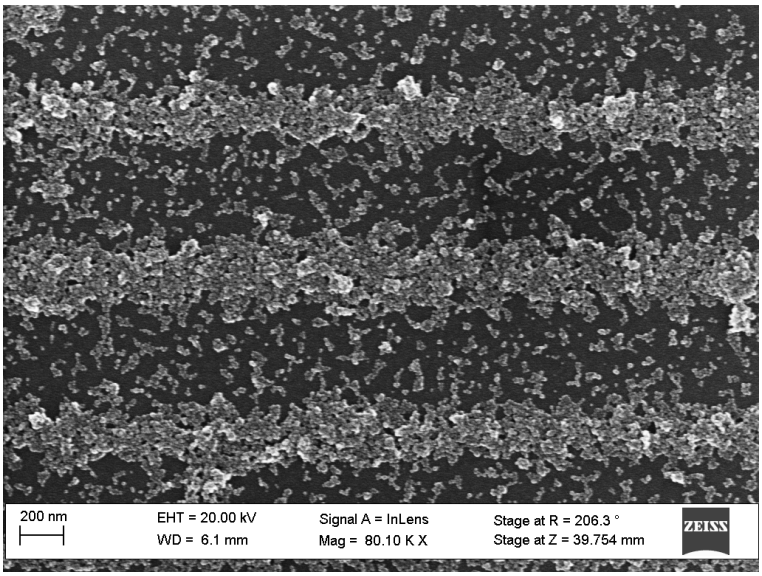

Figure 4.4 SEM image of coupon coated for 30 minutes

SEM image for 30 minutes is shown in Figure 4.4. The width growth in 30 minutes is almost twice of the width growth in 15 minutes.

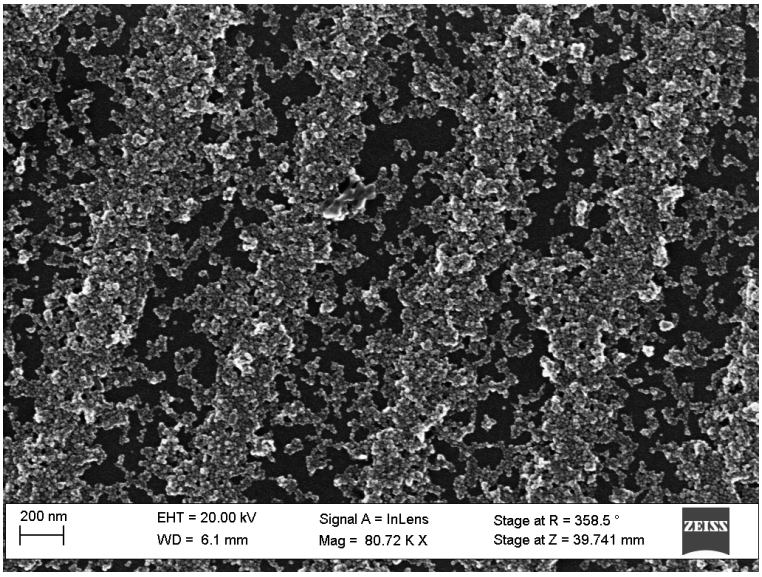

Figure 4.5 SEM image of coupon coater for 1 hour

For each sample more than 15 high resolution images with different magnification were taken, and all images were analyzed with "ImageJ" program.

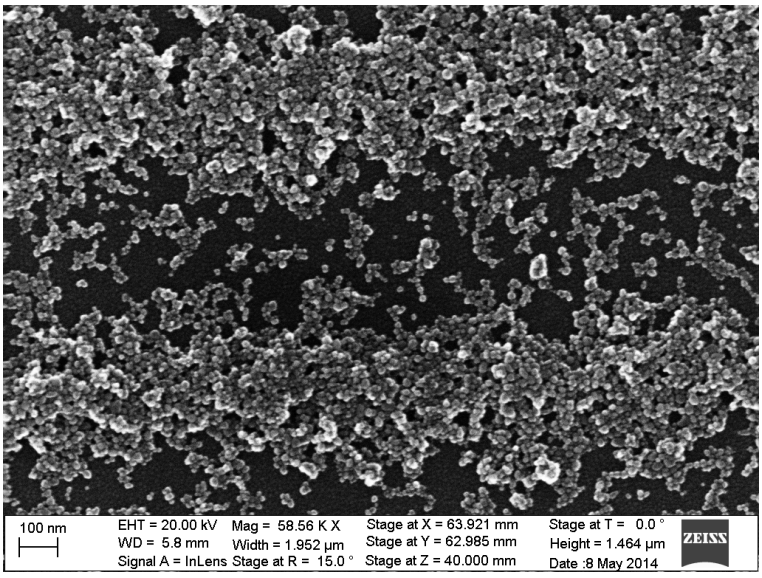

Figure 4.6 SEM image of coupon coated for 2 hours

Table 4.1 shows the calculated average width growth for different times.

Table 4.1 Average Width and standard deviation for different coating times

Time [min]	Average Width [nm]	SDEV [nm]
5	149	15.4×10^{-9}
15	158	12.68×10^{-9}
30	330	29.11×10^{-9}
60	462	26.53×10^{-9}
120	525	33.93×10^{-9}

These results suggest that for 5 and 15 minutes coating these coupons show similar width. However, the growth is different for 30 minutes coated coupon, about $330nm$. Also, in 1 hour coating particles grow about $462nm$, whereas in 2 hours they grow about $525nm$.

Clearly, nanoparticle patterns grow rapidly at short times and then growth slows for longer times. The table above shows the average width growth of nano particles arrays and related standard deviation for different coating times.

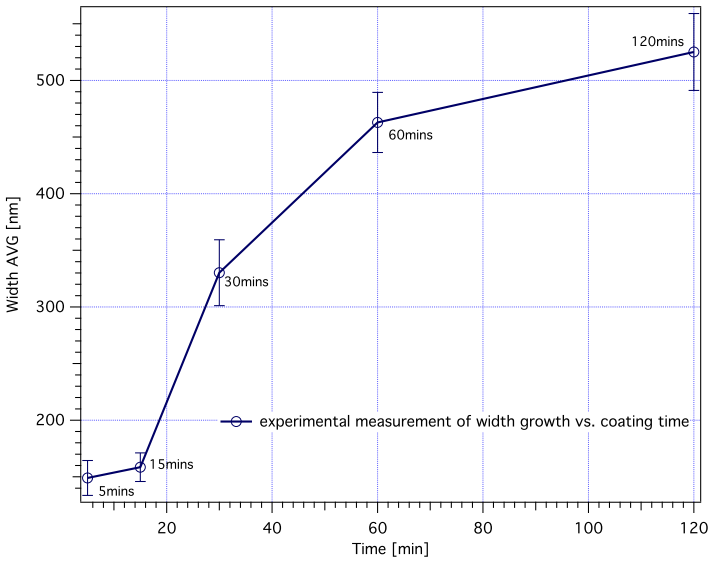

Figure 4.7 Change of width of arrays at different assembly times

The plot of average width growth of these data is shown in figure 4.7.

4.2 Pattern Height

SEM images suggest that nanoparticles not only grow in width, but also in height. We cannot determine the height with SEM. However, we can measure height with using Atomic Force Microscopy (AFM). Once again to obtain height difference coupon was coated 5 times for 5 different time intervals. For each coupon a special cantilever with 300kHz resonance frequency and $40N/m$ force constant was used and each coupon was scanned with 1024 pixel resolution in AC-Mode.

The figures below represent AFM images for different coating times. Figure 4.8 shows AFM image for 5 minute coating. In this image bright spots represent maximum height. Similar to SEM images there are gaps within the patterns. Also, particles and crystals between arrays are noticeable in AFM imaging.

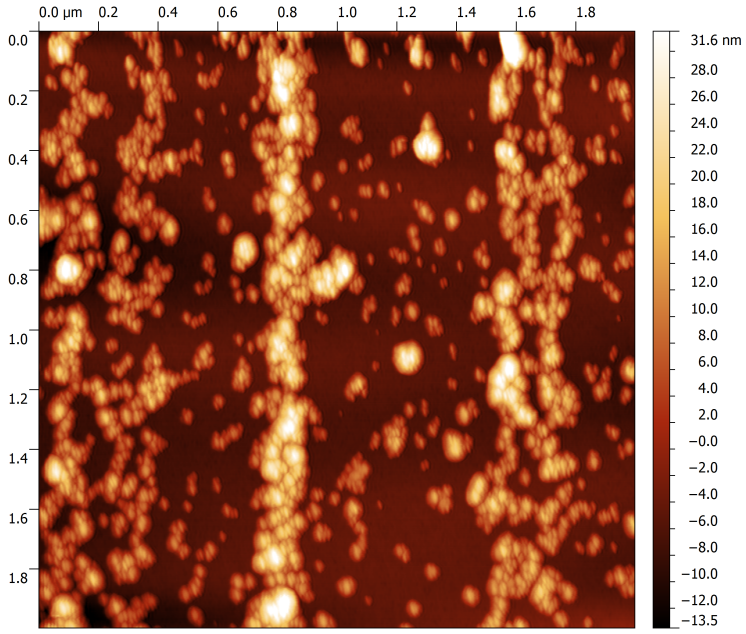

Figure 4.8 AFM image of coupon coated for 5 minutes

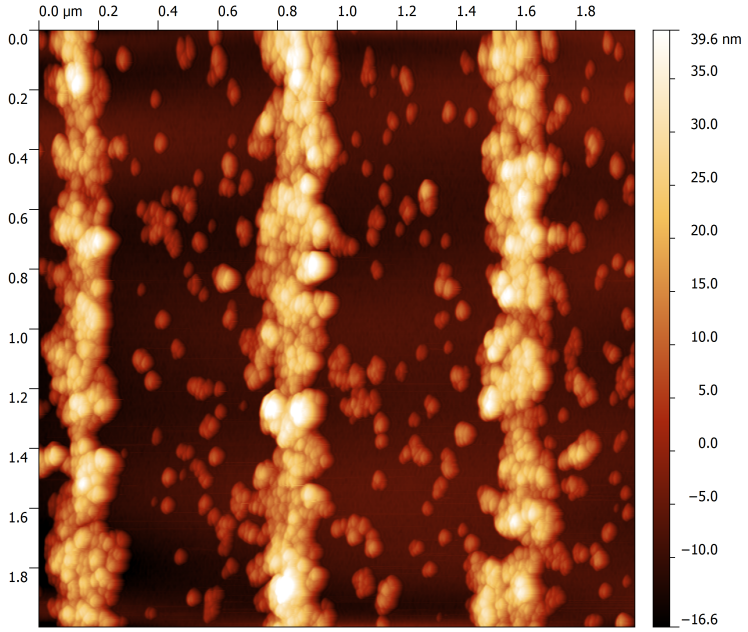

Figure 4.9 AFM image of coupon coated for 15 minutes

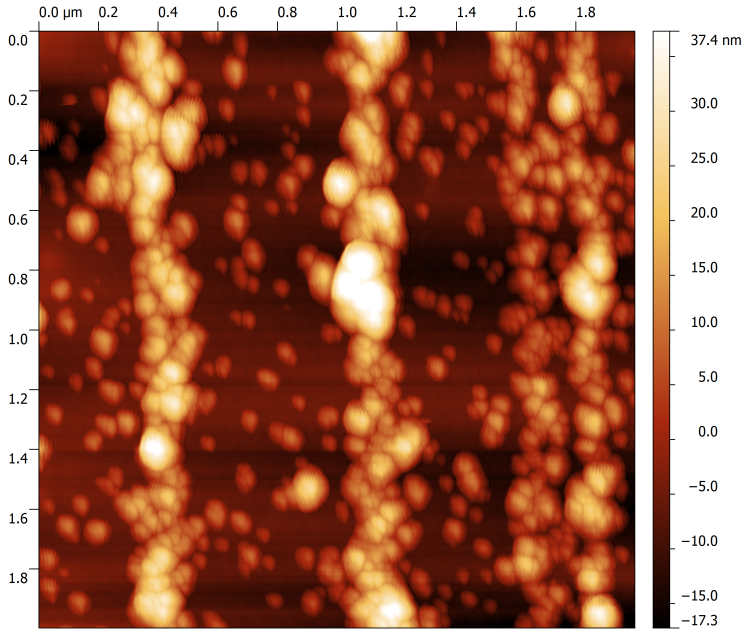

Figure 4.10 AFM image of coupon coated for 30 minutes

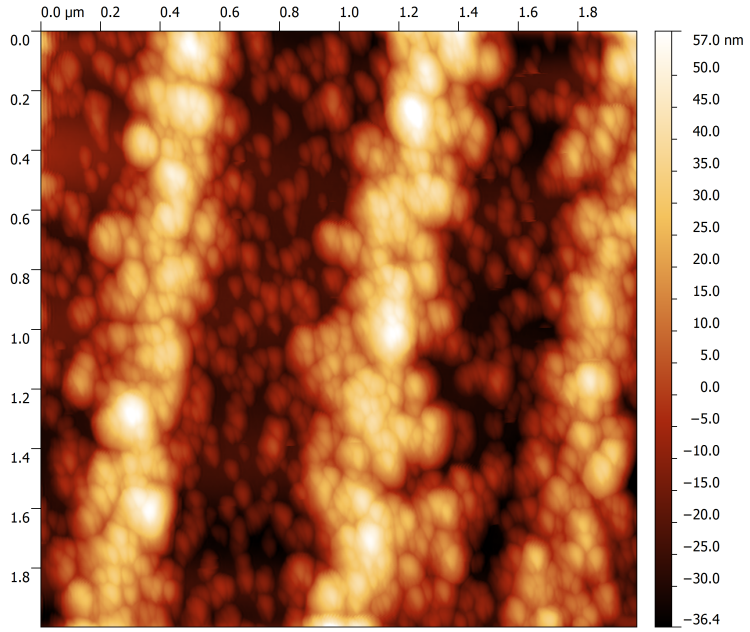

Figure 4.11 AFM image of coupon coated for 1 hour

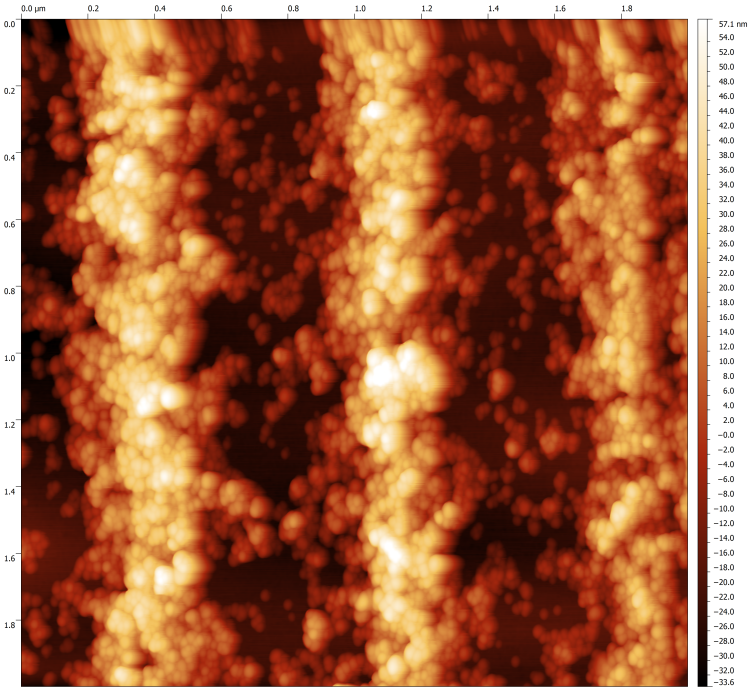

Figure 4.12 AFM image of coupon coated for 2 hours

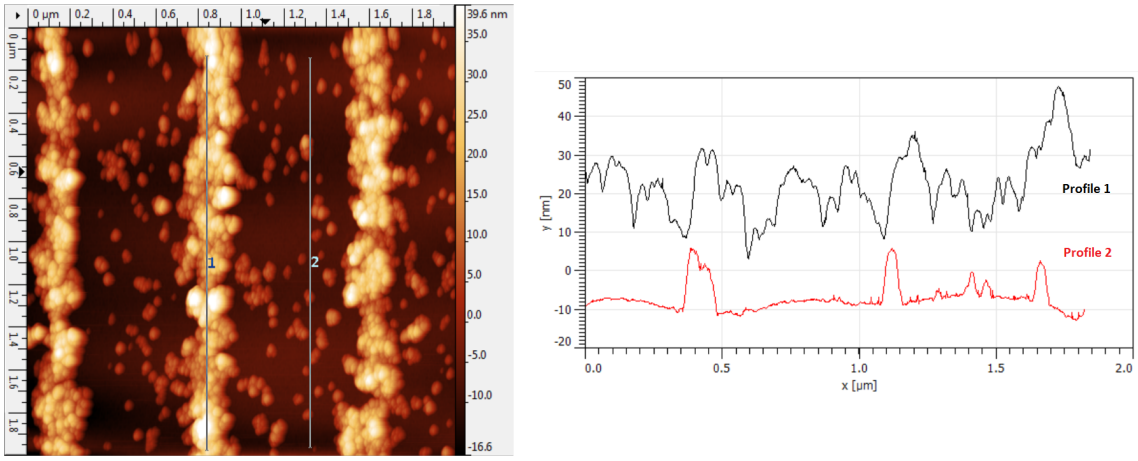

Figure 4.13 Vertical profiles on the pattern and empty space

The "Gwyddion" modular software was used to extract the background and analyze profiles in the AFM images. To get the average height, a set of vertical profiles were plotted together with the empty space between the patterns. Then average of empty space profiles was subtracted from pattern profiles. Figure 4.13 shows vertical profile on a pattern and on empty space.

The average height and related standard deviations are listed in table below.

Table 4.2 Average Height and standard deviation of different coating times

Time [min]	Average Height [nm]	SDEV [nm]
5	13.6	8.52×10^{-9}
15	21.4	9.8×10^{-9}
30	23.1	12×10^{-9}
60	36	12.6×10^{-9}
120	37	13.3×10^{-9}

Figure 4.14 shows average height as a function of coating time and Figure 4.15 shows related standard deviation for different times.

These data suggest that height growth also occurs, but patterns grow more horizontally than vertically. Width grows from about 149nm at 5 minutes to 520nm at 2hr, the height changes from 13nm at 5 minutes to 37nm at 2 hours. Thus, the aspect ratio changes from 10:1 at 5 minutes to 14:1 at 2 hours.

For coupon coated for 5 minutes, nanoparticles fill the transitions randomly and the height is about 1 nanoparticle whereas for 2 hours the height is about 3 nanoparticles. The reason why the standard deviation is higher for 2 hours than in 5 minutes can be due to aggregation of nanoparticles within the solution. In other words, in 5 minutes particles are not aggregated and each nanoparticle fills the transition line. However, in 2 hours not only single particles fill the transition lines but also small aggregated clusters of nano particles assemble themselves on other particles forming big valleys. This can be seen in Figure 4.16.

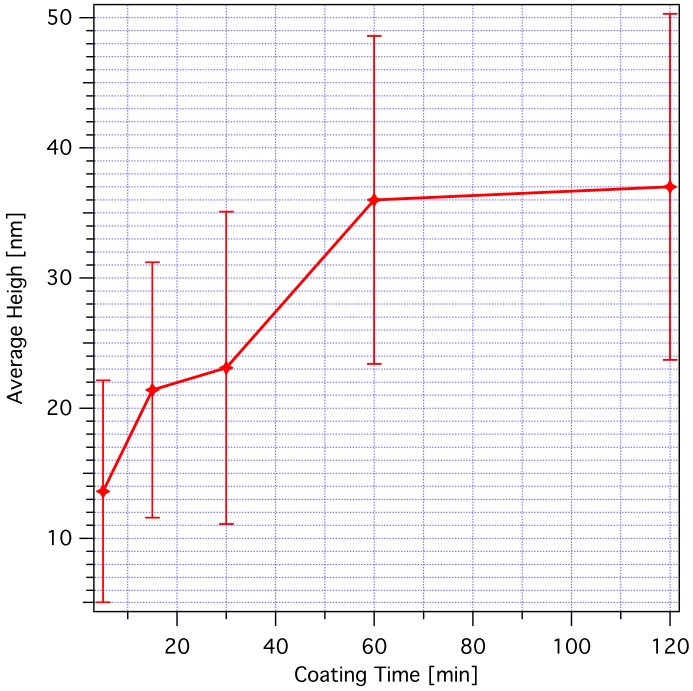

Figure 4.14 Change of height of arrays at different assembly times

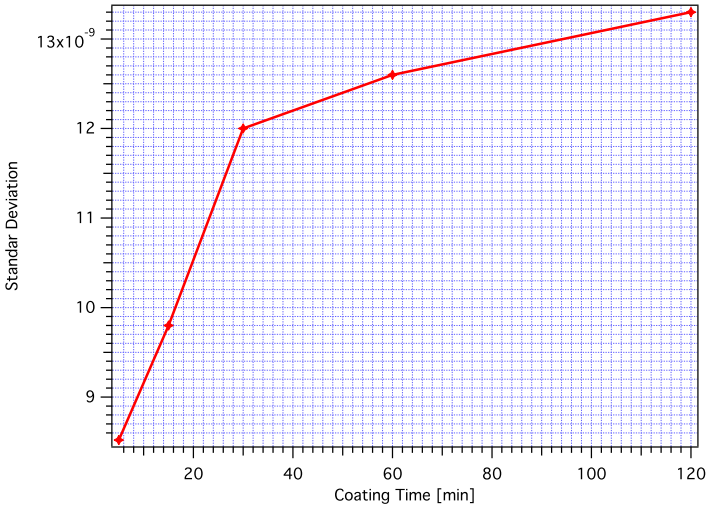

Figure 4.15 Plot of standard deviation as a function of assembly time

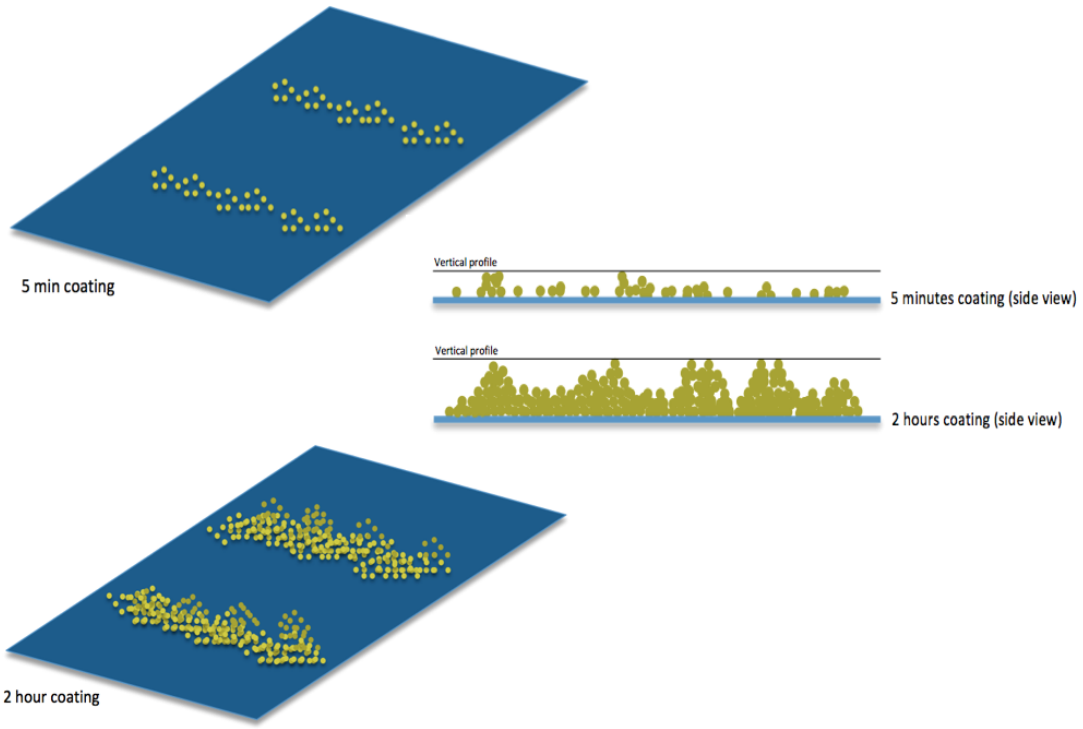

Figure 4.16 vertical profiles for 5 minutes coated coupon and 2 hours coated coupon

4.3 Magnetic Measurement of Nanoparticle Arrays

Once the nanoparticles are coated on the surface of the coupon, they are transferred by a polymer thin film and attached to quartz paddle. The quartz paddle is mounted to the VSM sample holder in order to study magnetic interactions in an external. Five samples with different coating times were made and cut into small pieces ($5mm^2$). Each sample is mounted in two different orientations: Lines perpendicular and parallel to the external field. We measured each sample twice, first from $-3000\ Oe$ to $3000\ Oe$ with $11\ Oe/sec$ is applied to see the change in magnetization hysteresis loops for each sample, and then a $50Oe$ range is scanned at $2\ Oe/sec$ to see the same when small field is applied. All measurements were done constant temperature $300K$.

Figure 4.17 shows normalized hysteresis loops for 5 different samples with external field of $3000\ Oe$ perpendicular to the patterns.

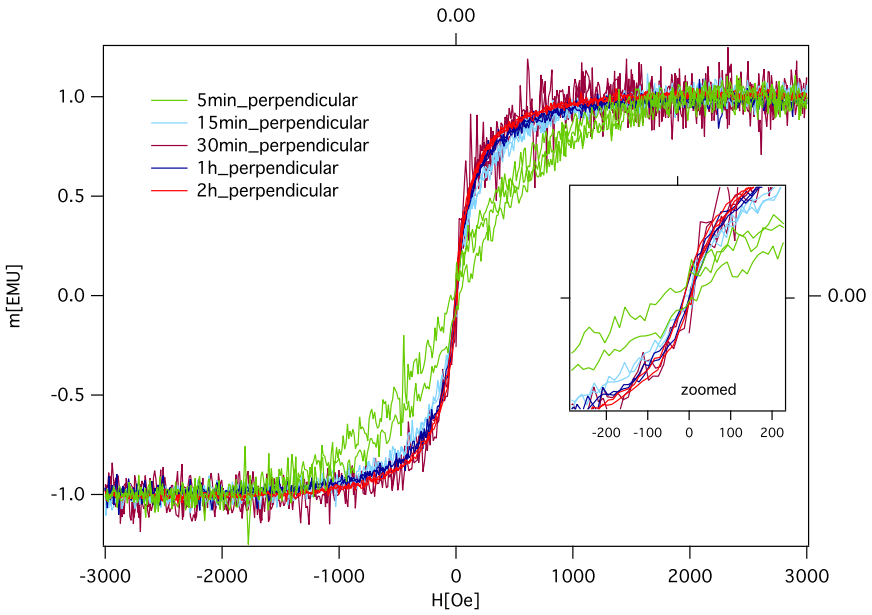

Figure 4.17 Normalized hysteresis plots for 5 samples oriented perpendicular to the external field

As shown in figure 4.17 the sample coated for 5 minutes has a different hysteresis loop than other 4 samples. It is also noticeable that sample with 2 hours is magnetized

with less field than all other samples.

Figure 4.18 shows normalized hysteresis loops for 5 different samples with external field of $3000Oe$ parallel to the patterns.

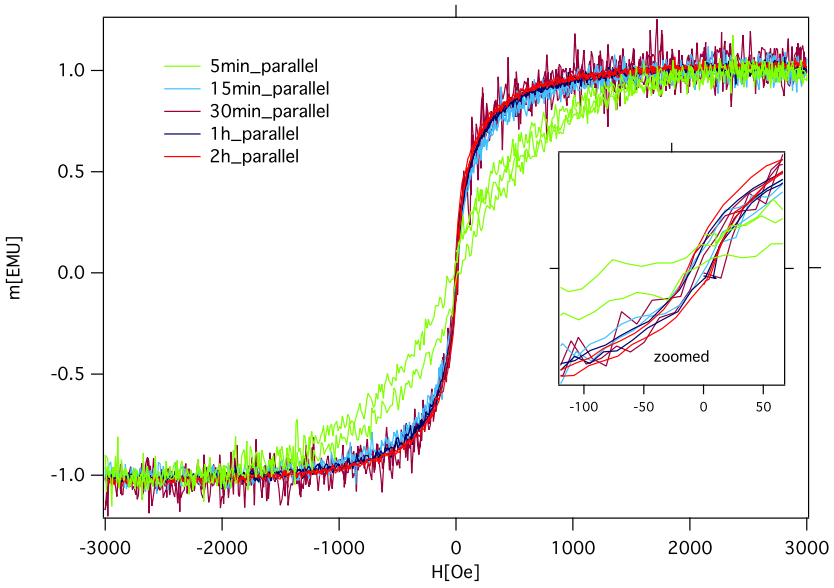

Figure 4.18 Normalized hysteresis plots for 5 samples oriented parallel to the external field

According to Figures 4.17 and 4.18, it appears that there is not a significant difference between perpendicular oriented and parallel oriented samples. Therefore, once the external field is applied there is more likely to be a local change; particle-particle interaction or cluster-cluster interaction.

To see the difference between hysteresis of perpendicular and parallel samples, it is better to plot perpendicular and parallel orientation for each sample together. Figures below show hysteresis for all 5 samples with perpendicular and parallel orientations.

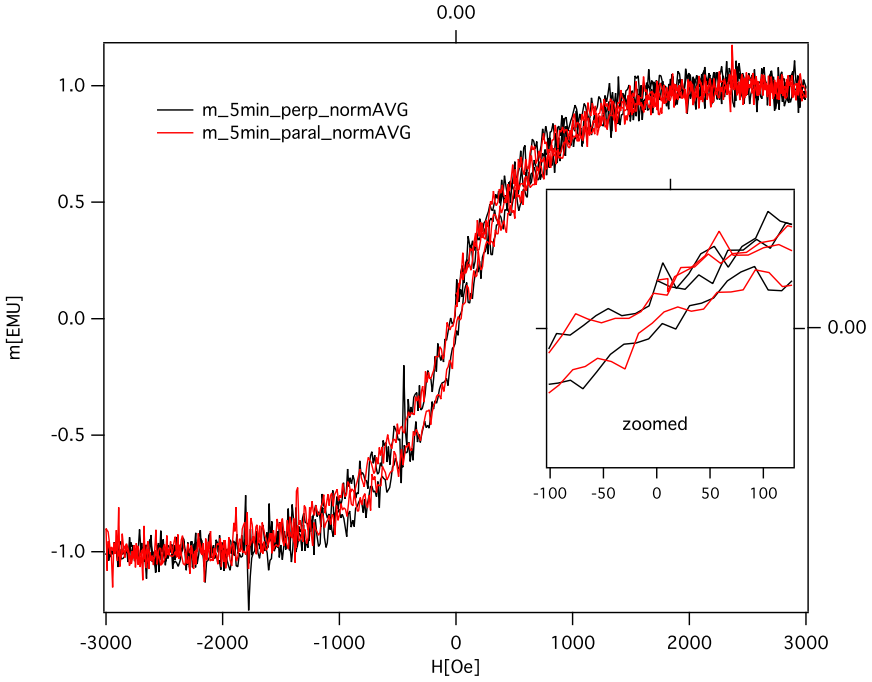

Figure 4.19 Perpendicular and parallel hysteresis for sample with 5 minutes coating time

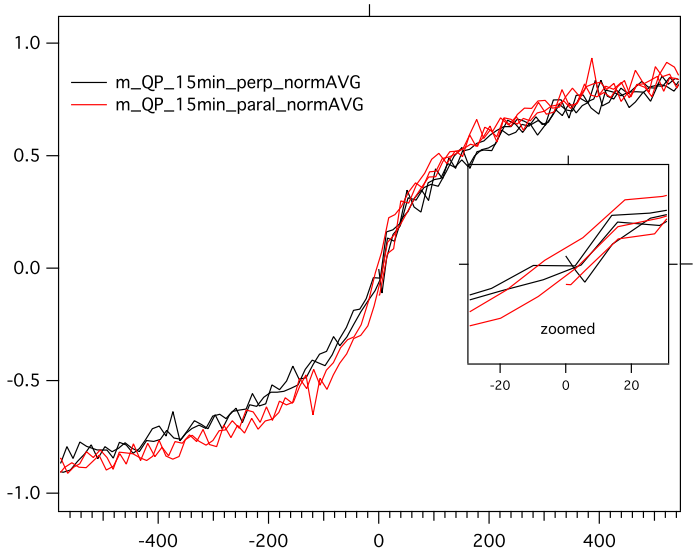

Figure 4.20 Perpendicular and parallel hysteresis for sample with 15 minutes coating time

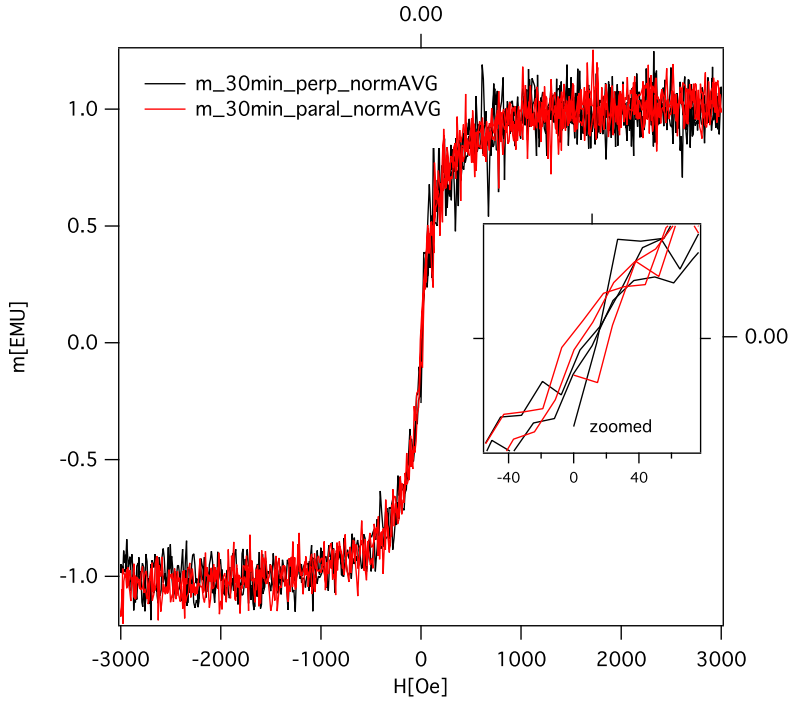

Figure 4.21 Perpendicular and parallel hysteresis for sample with 30 minutes coating time

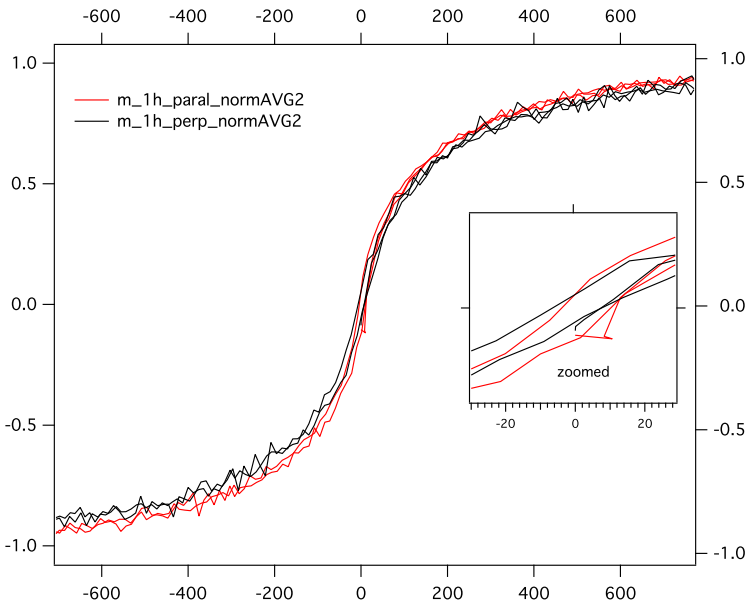

Figure 4.22 Perpendicular and parallel hysteresis for sample with 1 hour coating time

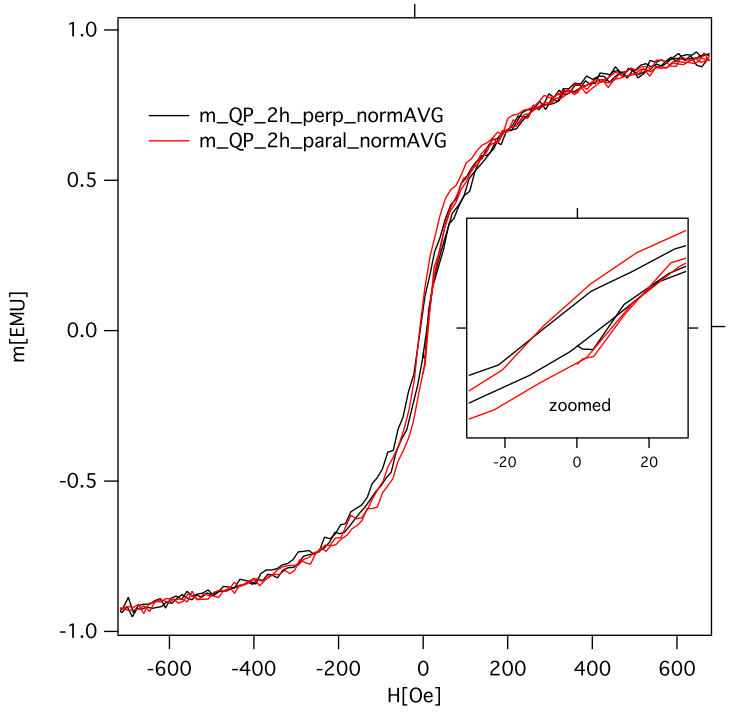

Figure 4.23 Perpendicular and parallel hysteresis for sample with 2 hours coating time

These plots show that parallel and perpendicular samples are same. Only for samples with higher coating time like 1 hour and 2 hours the magnetization is of a very small difference.

The difference between parallel and perpendicular cases can be analyzed by extracting Langevin Parameter "a" and fitting it to Langevin Equation (1.39).

$$M/M_0 = bH \tag{4.1}$$

In last equation, M_0 is saturation magnetization, M is magnetization at each field H and b is the constant number representing the slope of function, proportional to susceptibility, which also equals to $a/3$ in (1.39).

Constant "b" was extracted for two cases, $20Oe$ and $100Oe$. Average Values of b and related standard deviations for perpendicular and parallel cases are shown in table bellow.

Table 4.3 Calculated b parameter for perpendicular and parallel cases

Time [min]	b parallel	b perpendicular	SDEV parallel	SDEV perpendicular
5	0.0022432	0.0021931	0.00123	0.000521703
15	0.0062	0.0062	0.000578413	0.00255499
30	0.00862805	0.0064345	0.00585619	0.00133523
60	0.00938345	0.00713455	0.00496467	0.00297996
120	0.0106788	0.0079442	0.00602766	0.00340939

Figure 4.24 shows the plot of calculated data in table 4.3.

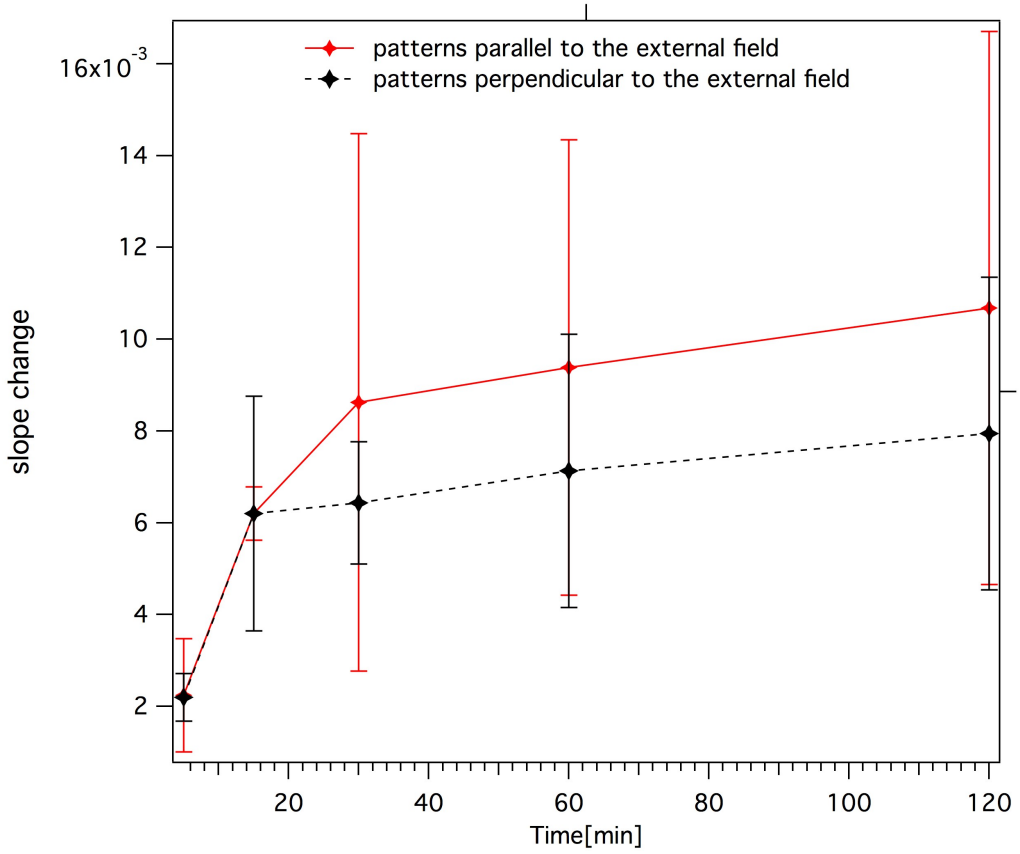

Figure 4.24 Change in slope of hystereses as a function of time

The coercivity for all cases is the same at room temperature. Figure 4.19 shows coercivity as a function of temperature for two different samples.

Magnetic hysteresis loops for sample with 15 minutes coating time was measured from $400K$ to $7K$, and for sample with 2 hours coating time was measured from $200K$ to $7K$. As seen in Figure 4.25, there is a difference in sample oriented perpendicular and parallel to the external field at $200K$-$50K$. This means, that pattern-pattern magnetic interactions is mostly noticeable at temperatures lower than $200K$.

4.4 Challenges Behind the Measurements

In experimental measurements it is hard to avoid errors.

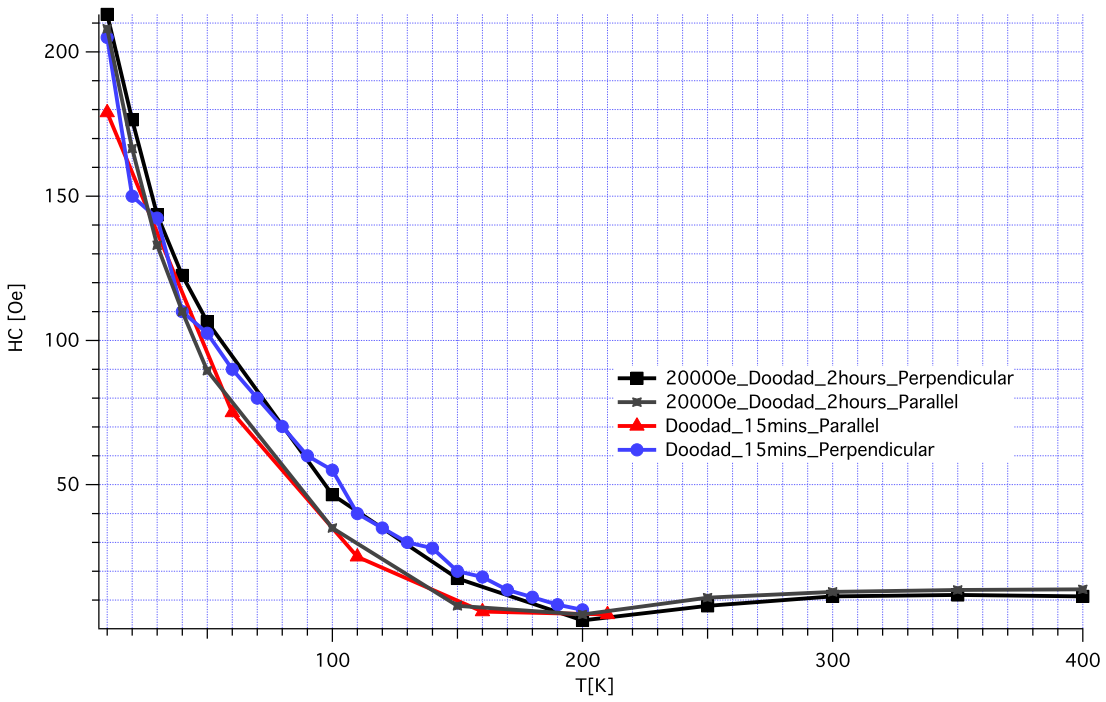

Figure 4.25 Coercivity as a function of temperature for 15 minutes and 2 hours coated samples

It is easy to get errors when dealing with nanoparticles, because in nanoscale a little bit of inaccuracy may cause a huge difference in calculations. The samples are attached to double sided tape. If the tape is touch by any metallic tool, it may attach tiny magnetic particles. This can cause a larger background once doing magnetometry.

The most challenging part of the measurement is the peeling process. Most of the time coated coupon is not totally peeled off. One reason can be DI water. DI water has to be inside a clean container and every time has to be checked for purity. Also, PVA as well as EMG707 particles have to be fresh and kept in a very clean place. EMG particles can easily get aggregated if the lid is open for long times.

4.5 Final Conclusion

Using SEM, AFM and VSM I studied magnetic-field directed self-assembly of magnetic nanoparticles into patterned arrays on the surface of perpendicular magnetic recording media. Results from imaging show that the average width and height increases as a function of coating time. Width of arrays varies with assembly time from 149nm at 5 minutes to 525nm at 120 minutes. Similarly, height changes from 13nm at 5 minutes to 37nm at 120 minutes. Therefore the pattern aspect ratio changes from 10:1 at 5 minutes to 14:1 at 120 minutes. For large widths compared with pattern spacing, the array interaction also causes a slope change in VSM hysteresis loops. While I hypothesize that as the patterns grow wider, the different regions (arrays) would interact with each other; however, what I actually observed appears to be more of a local change; particle-particle interaction. The hypothesis is not true yet because of the significant error bars. The other fact experiments suggest is that only for temperatures bellow $200K$ the difference between perpendicular and parallel samples is noticeable. There is a significant change in the slope or susceptibility for samples with 5 minutes and 2 hours of coating time (Figure 4.24). It is harder to magnetize samples with 2 hours of the coating time than the sample with 5 minutes of the coating time.This can be explained by the fact that in 5 minutes coating time, there are empty spots between particles within the patterns (Figures 4.2 and 4.8). Also, the increase in coating time suggests that there is a matching between change in the slope (susceptibility) and topographic plots (height and width); however, to prove it, one has to make a physical model in order to fit with the experimental data. SEM and AFM imaging also show that there are nano particles (or crystals) between arrays. Therefore, another suggestions for near future would be to find a way to reduce the number of particles between arrays and reduce the amount of PBS and repeat similar measurements.

Bibliography

[1] Sriharsha V. Aradhya et al. "Van der Waals interactions at metal/organic interfaces at the single-molecule level". In: *Nat Mater* 11.10 (Oct. 2012), pp. 872–876. URL: http://dx.doi.org/10.1038/nmat3403.

[2] Hans-Jürgen Butt, Brunero Cappella, and Michael Kappl. "Force measurements with the atomic force microscope: Technique, interpretation and applications". In: *Surface Science Reports* 59.1–6 (2005), pp. 1 –152. ISSN: 0167-5729. DOI: http://dx.doi.org/10.1016/j.surfrep.2005.08.003. URL: http://www.sciencedirect.com/science/article/pii/S0167572905000488.

[3] Lucija Coga, Stefano Masiero, and Irena Drevenšek-Olenik. "Lamellar versus compact self-assembly of lipoguanosine derivatives in thin surface films". In: *Colloids Surf B Biointerfaces* 121C (2014), pp. 114–121. DOI: 10.1016/j.colsurfb.2014.05.038.

[4] B. D. Cullity and C. D. Graham. *Introduction to Magnetic Materials*. John Wiley Sons, 2009, p. 544.

[5] Quantum Design. *Vibrating Sample Magnetometer (PPMS)*. 2009. URL: http://www.qdusa.com/sitedocs/appNotes/vsmappnote_5-09.pdf.

[6] Simon Foner. "Versatile and Sensitive Vibrating Sample Magnetometer". In: *Review of Scientific Instruments* 30 (1959), p. 548.

[7] J. I. Gittleman, B. Abeles, and S. Bozowski. "Superparamagnetism and relaxation effects in granular Ni-SiO_2 and Ni-Al_2O_3 films". In: *Phys. Rev. B* 9 (9 1974), pp. 3891–3897. DOI: 10.1103/PhysRevB.9.3891. URL: http://link.aps.org/doi/10.1103/PhysRevB.9.3891.

[8] *Hard Disk Longitudinal Recording*. URL: http://www.pctechguide.com/hard-disks/hard-disk-longitudinal-recording.

[9] *Hard Disk Perpendicular Recording*. URL: http://www.pctechguide.com/hard-disks/hard-disk-perpendicular-recording.

[10] J Henderson et al. “Pattern transfer nanomanufacturing using magnetic recording for programmed nanoparticle assembly”. In: *Nanotechnology* 23.18 (2012), p. 185304. DOI: 10.1088/0957-4484/23/18/185304.

[11] Charles Kittel. *Introduction to Solid State Physics*. Ed. by 8th. Wiley.

[12] R.W. Simmonds R. McDermott D.P. Pappas John M. Martinis K.M. Lang D.A. Hite. “Conducting atomic force microscopy for nanoscale tunnel barrier characterization”. In: *Review of Scientific Instruments* 75 (2004), pp. 2726–2731.

[13] F Einar Kruis, Heinz Fissan, and Aaron Peled. “Synthesis of nanoparticles in the gas phase for electronic, optical and magnetic applications—a review”. In: *Journal of Aerosol Science* 29.5 (1998), pp. 511–535.

[14] Magda Latorre and Carlos Rinaldi. “Applications of magnetic nanoparticles in medicine: magnetic fluid hyperthermia”. In: *Puerto Rico health sciences journal* 28.3 (2009).

[15] T.C Lim. “The Relationship between Lennard-Jones (12-6) and Morse Potential Functions”. In: *Zeitschrift fur Naturforschung - Section A Journal of Physical Sciences* 58.11 (2002), pp. 615–617.

[16] *Magnetic Recording Theory*. URL: https://ccrma.stanford.edu/courses/192a/6-Magnetic_Recording.pdf.

[17] *Scanning Electron Microscopy Technology, Scanning Electron Microscopy Technology Overview*. 2014. URL: http://www.nanoscience.com/products/sem/technology-overview/.

[18] Andrew N Shipway, Eugenii Katz, and Itamar Willner. “Nanoparticle arrays on surfaces for electronic, optical, and sensor applications”. In: *ChemPhysChem* 1.1 (2000), pp. 18–52.

[19] *The Lennard–Jones potential*. 2000. URL: http://cps-www.bu.edu/Wasser/robert/work/node8.html.

[20] J. C. Scaiano Turro Nicholas J and V. Ramamurthy. *Principles of Molecular Photochemistry : An Introduction*. Palgrave, 2008.

[21] *Vibrating Sample Magnetometer (VSM) Option Vibrating Sample Magnetometer (VSM) Option Vibrating Sample Magnetometer (VSM) User's Manual*. Quantum Design. 6325 Lusk Boulevard San Diego, CA 92121 USA, 2011.

[22] Shan X. Wang and Alexander M. Taratorin. *Magnetic Information Storage Technology*. Academic Press, 1999.

[23] L. Ye et al. "All-nanoparticle concave diffraction grating fabricated by self-assembly onto magnetically-recorded templates". In: *Opt. Express* 21.1 (2013), pp. 1066–1075. DOI: 10.1364/OE.21.001066. URL: http://www.opticsexpress.org/abstract.cfm?URI=oe-21-1-1066.

[24] L Ye et al. "Magnetic field gradient driven self-assembly of superparamagnetic nanoparticles using programmable magnetically-recorded templates". In: *APS Meeting Abstracts*. Vol. 1. 2013, p. 32002.

[25] Lisha Zhang et al. "Nanoparticles in medicine: therapeutic applications and developments". In: *Clinical Pharmacology & Therapeutics* 83.5 (2007), pp. 761–769.